July 2019

The Climatic and Hydrostratigraphic Controls on Brine-to-Freshwater Interface Dynamics in Hyperarid Climates: A 2-D Parametric Groundwater Modeling Study

Sarah McKnight
University of Massachusetts Amherst

The Climatic and Hydrostratigraphic Controls on Brine-to-Freshwater Interface Dynamics in Hyperarid Climates: A 2-D Parametric Groundwater Modeling Study

A Thesis Presented

by

SARAH V. McKNIGHT

Submitted to the Graduate School of the
University of Massachusetts Amherst in partial fulfillment
of the requirements for the degree of

MASTER OF SCIENCE

May 2019

Department of Geosciences

The Climatic and Hydrostratigraphic Controls on Brine-to-Freshwater Interface Dynamics in Hyperarid Climates: A 2-D Parametric Groundwater Modeling Study

A Thesis Presented

By

SARAH V. McKNIGHT

Approved as to style and content by:

David F. Boutt, Chair

Michele Cooke, Member

Jon Woodruff, Member

Julie Brigham-Grette, Department Head
Department of Geosciences

ACKNOWLEDGEMENTS

I would first like to thank my advisor, Dave Boutt, who has been a tireless and diligent mentor. I deeply appreciate his efforts. I would also like to thank our colleague LeeAnn Munk at the University of Alaska, who has provided guidance and valuable knowledge on the geology of Salar de Atacama.

Much gratitude also goes out to Professor Michele Cooke and Professor Jon Woodruff, who reviewed drafts of both my proposal and my thesis and provided critical feedback through the review process.

To my dear family and friends, thank you for your endless patience, and thank you for your positive energy in my life.

Many thanks to Albemerle for sharing their data and information on Salar de Atacama and for providing continuous support in our team's research efforts.

ABSTRACT

CLIMATIC AND HYDROSTRATIGRAPHIC CONTROLS ON BRINE-TO-FRESHWATER INTERFACE DYNAMICS IN HYPERARID REGIONS: A 2-D PARAMETRIC GROUNDWATER MODELING STUDY

MAY 2019

SARAH V. McKNIGHT, B.A., MOUNT HOLYOKE COLLEGE

M.S., UNIVERSITY OF MASSACHUSETTS AMHERST

Directed by: Prof. David F. Boutt

Density dependent flow occurs in areas where high-salinity groundwater interacts with low-salinity groundwater to create a brine-to-freshwater interface that defies common assumptions about groundwater movement. Yet the geologic and hydrologic factors that impact interface dynamics and migration remain poorly defined. With less than 20 $mm \bullet yr^{-1}$ of precipitation and with an extremely dense (i.e. 1.2 $g \bullet cm^{-3}$) naturally occurring brine, Chile's Salar de Atacama (SdA) provides an excellent analog for exploring interface dynamics in other arid regions. Site-specific 2-D models of the interface in the southeastern region of SdA, with interpretations of the hydrostratigraphic framework, provide an analysis for density-driven response rates to climatic change. A separate parametric, equally probable series of distributions of hydraulic conductivity provides a means for expanding analysis to other similar arid salar (i.e. "salt flat") environments. Comparing the modeled interface's geometry and response to perturbations in the rates of lateral recharge in each hydrostratigraphic realization yields insight into the dynamics of interface migration to coupled climatic and geologic conditions. Changes in hydrologic conditions, informed by paleoclimatic interpretations and previously modeled climate predictions, are introduced to each hydrostratigraphic realization following the interface reaching an initial dynamic equilibrium, and the interface's response is assessed subsequent to it reaching

a new dynamic equilibrium. Metrics for model evaluation include migration rate, change in the interface's areal extent, change in interface slope, and the response rate following the introduction to a perturbation in the aquifer's hydrology. Model analyses suggest that evaporation rates strongly control the interface's geometry and sensitivity despite climatic and geologic conditions; continuity of high-permeability pathways controls interface slope; increasing continuity also decreases interface stability in terms of time required to reach a new steady state. While these results have implications for interface dynamics in both salars specifically and arid climates in general, they also indicate the importance of considering hydrostatigraphic continuity for saline water intrusion in coastal regions. They also provide a compelling method for assessing interface dynamics in other climatic and geologic conditions.

Highlights:

1.) Increasing horizontal continuity of hydrostratigraphic units generally decreases the slope of brine-to-freshwater interfaces;

2.) Increasing continuity also increases the sensitivity and decreases the stability of interface migration in response to climate-based changes in recharge in an arid basin;

3.) Evaporation presents a controlling factor on the geometry of the interface in the upper unconfined aquifer where ET overlaps with the interface's confluence with the surface.

PREFACE

This thesis evaluates the hydrologic and geologic controls on brine-to-freshwater interface dynamics in arid climates through a manuscript format that comprises a main body of text describing analytical methods and findings. Supplemental material provides additional information on the genesis of SdA's hydrostratigraphic framework and sensitivity analyses for the numerical model's boundary conditions. I led the writing and analysis on the manuscript with significant contributions from Dr. David Boutt (University of Massachusetts Amherst) and Dr. LeeAnn Munk (University of Alaska Ancorage). Figures and tables provided here for the manuscript have been separated out into supplemental material for the manuscript format requirements for peer-reviewed journals.

TABLE OF CONTENTS

LIST OF TABLES

Table Page

LIST OF FIGURES

Figure Page

CHAPTER 1

CLIMATIC AND HYDROSTRATIGRAPHIC CONTROLS ON BRINE-TO-FRESHWATER INTERFACE DYNAMICS IN HYPERARID REGIONS: A 2-D PARAMETRIC GROUNDWATER MODELING STUDY

1.1 Abstract

Accurately defining the geometry and the transient dynamics of brine-to-freshwater interfaces in brine-bearing aquifers has critical implications for estimating the risk of saline intrusion on potable water resources and the sustainability of groundwater-fed ecosystems, which are both common concerns in arid regions. Yet density-driven numerical flow models fail to capture the geometry of interfaces when relying on homogenous hydraulic frameworks. We show that geologic heterogeneity in numerical simulations of density-driven groundwater flow impact the timing and migration of the brine-to-freshwater interface in response to changes in subsurface lateral inflow. We utilize lithologic data to create both a hydrostratigraphic framework, which is a distribution of hydraulic conductivity based on a geologic interpretation, and three sets of geostatistical realizations of hydraulic conductivity distributions with different ratios of horizontal to vertical continuity. We then expose each model to changes in simulated inflow to assess their geometry and time-sensitive response. Results from the simulations exhibit trends with changes in horizontal continuity, including a decrease of the interface's slope that increasingly match field observations from Salar de Atacama. With increasing horizontal hydrostratigraphic continuity, brine-to-freshwater interfaces also express increasing sensitivity in terms of distance that the interface travels and decreasing stability in terms of the amount of time required for an interface to cease migration. Results suggest that density-driven circulation produces dynamic responses to hydrologic changes that cannot be accurately predicted by

geologically unrealistic homogenous models. Results further implicate the risk of groundwater-fed ecosystems that rely on aquifers with saline intrusion issues, based on the common reliance on homogenous or simple layered groundwater flow simulations. This sensitivity analysis represents the first attempt to constrain the impact stratigraphic continuity and geologic complexity on saline intrusion dynamics in a brine-to-freshwater interface's response to climate-driven changes in subsurface lateral recharge.

1.2 Introduction

Predictions of density-driven flow that occurs during saline versus fresh groundwater interactions are based on analytical equations from simple physics. Numerical simulations of density-driven groundwater flow through porous media indicate that high density brine (i.e. 1,200 kg/m^3) and lower density freshwater (i.e. 1,000 kg/m^3) interactions create an interface between the two distinct fluids with different densities. The interface meets the surface, commonly at an area of discharge, and dips downward toward the direction of freshwater flow to create a freshwater lens overlying a highly saline brine. In simulations with homogenous and isotropic hydraulic conductivity, the slope of the interface's dip is approximately 1:1 in horizontal to vertical distance, or about 45°-56° from horizontal [*Fan et al.*, 1996; *Langevin and Guo*, 2006].

Yet field observations consistently defy theory-based predictions in endorheic basins. Specifically in Salar de Atacama (SdA) in northern Chile, we document the presence of a brine-to-freshwater interface that is extraordinarily shallow (1-3°) and is difficult to model under homogenous conditions (Figure 1). Marazuela et al. (2017) also document the interface geometry along the eastern margin of SdA, finding similarly shallow slopes but also being unable to capture that geometry using either a homogenous model or a simplistic model of changing

hydraulic conductivity (HK; Figure 1). While introducing anisotropy of hydraulic conductivity decreases the interface slope, such simulations remain insufficient in accurately predicting observed values. We therefore aim to analyze the impact of subsurface heterogeneity via HK on the geometry of the interface in order to simulate more accurate salt concentration values in groundwater, and we further aim to investigate how subsurface heterogeneity effects the time-dependent response of the interface to changes in recharge. Brine-bearing aquifers in arid environments and coastal regions host groundwater-fed ecosystems that both rely on the interface's location and are threatened by its potential movement. Developing accurate numerical simulations of interface geometry and dynamics is therefore critical for accurate predictions of saline groundwater intrusion and ecosystem sustainability in response to changes in hydrology.

Endorheic basins often contain brine-bearing aquifers with saline migration risks that remain poorly understood. While saline fluid circulation is a ubiquitous feature in coastal environments (Konikow et al., 2013), and previous studies extensively document coastal saline water intrusion's risk to potable resources (Heiss & Michael, 2014; Konikow et al., 2013; Meng et al., 2002; Sawyer et al., 2014; Trabelsi et al., 2013), density-driven circulation also commonly occurs in endorheic basins in arid climates, where high evaporation rates outpace recharge and thus develop high-density subsurface brine (Anderson et al., 2002; Houston et al., 2011; Vásquez et al., 2013). Endorheic basins account for approximately 20% of total land area in the world, and they also contribute to the equivalent sea level rise of almost half of land-based glacier melt, and thus endorheic basins are a vital component of the hydrologic cycle (Wang et al., 2018). Arid, endorheic basins also have hydrologic conditions, such as inconsistent surficial recharge and high rates of evaporation, that can be unique from coastal environments and impact both mining and freshwater resources as well as environmental interests (Duffy & Al-Hassan, 1988).

However, interfaces in arid environments remain poorly understood in terms of how geologic complexity impacts density-driven fluid dynamics in response to changes in recharge to the aquifer. Constraining the impact of geologic complexity on brine-to-freshwater interface dynamics in arid basins is crucial for forecasting saline groundwater migration, which is the movement of the interface between the freshwater and brine that results from a change in the aquifer's hydraulic field. Endorheic basins provide an excellent opportunity to study how subsurface heterogeneity influences a brine-to-freshwater interface's geometry and dynamics without the complicating factors of tidal influence and groundwater-to-ocean discharge. Salars are salt flats ("playas") that commonly develop in arid basins as a result of discharge outpacing recharge rates via evaporation. This evapoconcentration process develops low-permeability evaporite sequences that commonly interbed with higher-permeability lithologies [*Rosen et al.*, 1994], and therefore salars are also particularly ideal for assessing fluid dynamics of preferential pathways that develop in geologically complex strata.

While previous studies have identified geologic factors such as stratigraphic continuity (Michael et al., 2016) and media permeability (Russoniello et al., 2013) as significant contributors to interface geometry under static conditions, the transient reaction and stability of brine-to-freshwater interfaces as a result of subsurface heterogeneity remain unconstrained. Discharge via evapotranspiration from groundwater-fed wetlands also provide the main if not the only location for groundwater-surface water exchange in arid, endorheic basins (Tyler et al., 2006). However, no studies have evaluated the impact of focused discharge via evapotranspiration on the sensitivity and stability of interfaces that frequently develop in association with wetlands in arid, endorheic basins, despite the documented global decline in saline lakes (Wurtsbaugh et al., 2017). Along with the dynamic response of an interface to

changes in recharge, specifically for arid, endorheic basins, there are limited constraints on the factors that control the geometry of interfaces. Subsurface heterogeneity in HK values shallows interface geometry and delays responses to hydrologic changes when compared to homogenous simulations, and this impact therefore requires further investigation. Thus, this study expands on the analysis of heterogeneity under modeled arid climate conditions and further analyzes interface sensitivity to varying geologically heterogeneous conditions and recharge rate changes.

To understand how subsurface heterogeneity in HK influences both the geometry and the dynamic response of interfaces in arid, endorheic basins, a series of numerical models simulate an interface's time-sensitive response to changes in recharge under different hydraulic conditions. One model represents a heterogeneous distribution of HK based on the hydrostratigaphic framework for SdA, in which the HK values reflect the interpreted geology of the area (S2), while a second model represents the homogenous equivalent with the same effective hydraulic conductivity (K_{eff}) as the hydrostratigraphic framework. Lithologic information from 28 cores in the southeastern margin of SdA constrains the hydrostratigraphic framework. Another separate set of realizations of hydraulic conductivity is based on SdA's geology and corresponding hydraulic test data, which is further described in the supplementary section S2. By assigning specific hydraulic properties to the lithologies represented in the core data, it is possible to assess the role of subsurface heterogeneity on interface dynamics via density-driven numerical simulations. The purpose of the simulations representing different realizations of hydraulic conductivity is to generalize the impact of hydraulically conductive pathways on interface sensitivity and stability to basin-scale hydrologic changes. The observations of the realizations will provide insight on how continuity may impact the

differences in interface geometry and dynamics between the heterogeneous and the homogenous distributions of hydraulic conductivity for SdA.

With the above-described approach, we employed a series of metrics to assess the geometry and dynamic response of the interface to changes in recharge. Since the real conditions can only be compared to simulations of site-specific distributions of hydraulic conductivity, we address the plausibility of modeled conditions for SdA-specific simulations by comparing computed versus simulated values, as well as comparing the location of the simulated 0.5 isoconcentration curve with the observed interface. For all simulations, a comparison of interface geometry and dynamic response under different modeled conditions provides insight into how subsurface heterogeneity influence interfaces geometry and dynamics in arid, endorheic basins. Metrics for assessing the interface geometry for all simulations include slope, transition zone thickness, and qualitative characterization. Assessments of the interface's dynamic response to hydraulic changes include distance of migration and time required to reach stability. The findings from this work have implications for saline migration in increasingly arid climates as well as potable water development, groundwater-fed ecosystem sustainability, and brine resource extraction in arid, endorheic basins.

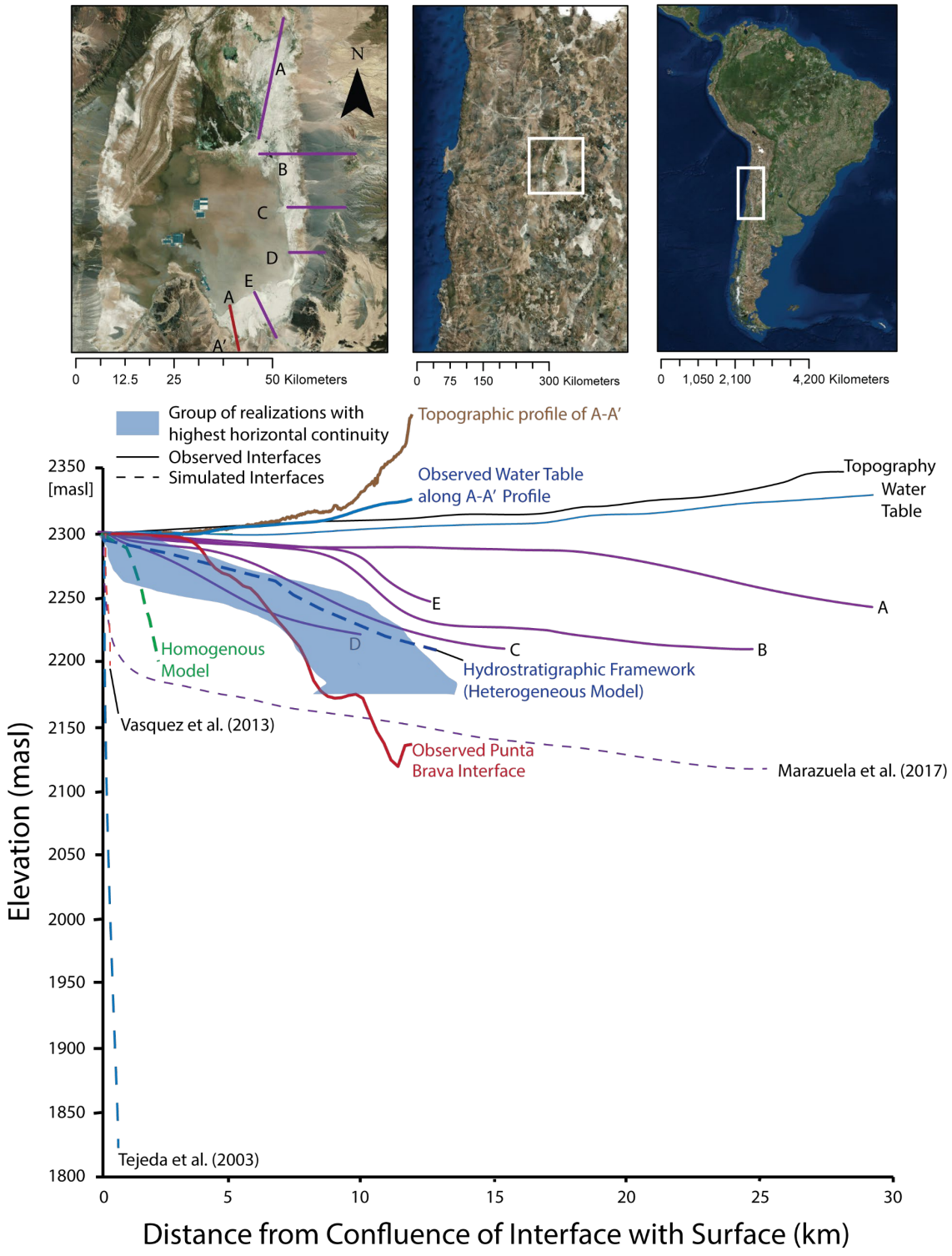

Figure 1 Comparison of observed 2-D interface locations with numerical simulations (dashed lines) of the interface along the transitions zone of Salar de Atacama. Observed interfaces A-E (purple solid lines) are extracted from Marazuela et al. (2017) with locations along the eastern margin of the salar, as seen in the reference map in the upper left corner. The observed interface for this study along the A-A' transect is the solid red line.

1.3 Background

1.3.1 Hydrogeologic conditions of interfaces between fluids with varying densities

Variation in solute concentration results in varying density among subsurface fluids. This discrepancy creates density-dependent flow, which results in subsurface fluid convection and develops an interface between fluids with distinct densities (Heiss & Michael, 2014; Philip & van Duijn, 1996). For coastal areas, such interfaces have been extensively documented [*Yechieli et al.*, 2001; *Werner and Simmons*, 2009; *Trabelsi et al.*, 2013]. However, for interfaces located in inland basins, the processes that control the geometry of continental interfaces remain unconstrained [*Tejeda et al.*, 2003; *Vásquez et al.*, 2013]. In most cases, the extreme discrepancy in fluid density encourages the development of an interface where the denser brine underlies the less dense fluid [*Duffy and Hassan*, 1988; *Fan et al.*, 1996; *Wooding et al.*, 1997; *Houston et al.*, 2011]. As stated by the Ghyben-Herzberg model [*Morgan et al.*, 2012], an increase in the density discrepancy between two distinct fluids will decrease the slope of the interface (Yoseph Yechieli, 2000).

Previous studies contend that an interface's geometry and migration depends on multiple hydrologic and geologic factors (Houston, 2009; Tejeda et al., 2003). However, the degree to which these factors impact interface dynamics, the change in fluid flow that results in brine-to-freshwater interface movement, remains poorly defined. Stratigraphic units' hydraulic conductivity increases saline groundwater circulation [*Konikow et al.*, 2013], but it is unclear to what degree basin-scale hydrostratigraphic complexity influences interface development when compared to the aquifer's distribution of recharge and discharge mechanisms (Houston et al., 2011).

Upwelling of freshwater caused by density-dependent flow creates groundwater-fed surface water bodies [*Ortiz et al.*, 2013], which are critical points of surface water-groundwater exchange in arid basins [*Tyler et al.*, 2006]. The surface water bodies also serve as a primary point for evaporative concentration, which is the main mechanism of brine development in arid basins, both in northern Chile [*Risacher et al.*, 2013] and throughout the world [*Fan et al.*, 1996].

Thus, surface water bodies are a common feature of interface hydrogeology and represent a critical component to both discharge and recharge in brine-rich aquifers. Better understanding the hydrologic factors that influence interface geometry and movement therefore informs basic-scale hydrologic budgets for brine-bearing aquifers. Constraining the conditions that impact the geometry and migration of interfaces are also important for both groundwater resource estimation and groundwater-fed wetlands conservation. Better predictions of interface dynamics will enhance the future productivity of aquifer development.

1.3.2 Dynamic response of brine-to-freshwater interfaces

Studies frequently investigate the geometry and response of brine-to-freshwater interfaces along coastal areas. Literature about density-dependent interface dynamics in coastal areas primarily focuses on the impact of climate change on saline groundwater intrusion [*Meng et al.*, 2002; *Werner and Simmons*, 2009; *Liu et al.*, 2014]. Intrusion from increasing sea level and tidal fluctuations threatens potable water sources and thus provides the main motivation for these studies (Bailey, 2015; Heiss & Michael, 2014; Trabelsi et al., 2013). While studies of saline groundwater intrusion primarily focus on coastal environments, that same focus does not extend to inland, arid basins despite their prevalence and unique conditions. Such aquifers tend to exhibit variably sharp to diffuse interface between fresh and saline fluids (Herrera et al., 2016) and a relatively shallow slope (Yoseph Yechieli, 2000) due to the high density discrepancy

between brine and freshwater when compared to seawater. Such arid basins also lack the tidal influence exhibited in coastal environments and also experience high rates of evaporation [*Hernandez-Lopez et al.*, 2006] and exhibit lateral subsurface inflow as the long-term dominant recharge mechanism [*Montgomery et al.*, 2003].

Studies on the interface dynamics of brines in arid basins have focused on the interface's geometry and migration under either homogenous hydraulic conductivity conditions [*Tejeda et al.*, 2003] or simplistic stratigraphic interpretations with single-layer changes in hydraulic conductivity [*Duffy and Hassan*, 1988; *Marazuela et al.*, 2019]. Playa environments can develop a wide range of stratigraphically complex aquifers because their climate-sensitive change in areal extent can create a series of interbedding lithologies [*Houston et al.*, 2011]. For example, time periods with higher rates of recharge and precipitation will lead to increases in the areal extent of evaporite deposition, while lower rates will lead to a decreased extent within a basin. Since brine-bearing aquifers also commonly exist in tectonically active endorheic basins (Yager et al., 2017), faulting among lithologies further complicates the subsurface heterogeneity of hydraulic conductivity by introducing more lateral heterogeneity. Interfaces can exhibit variable behavior that defies theory when intersecting fault systems (Y. Yechieli et al., 2001), and thus the heterogeneity that faulting produces merits analysis in how it impacts density-driven flow along an interface. Modeling efforts have not yet considered possible heterogeneous interpretations of hydrostratigraphic aquifer conditions in arid basins specifically. Michael and Khan (2016) detail the effects of heterogeneity on solute transport through an aquifer while Michael et al. (2016) assess saline groundwater migration in the context of coastal conditions and provide an intensive analysis on the geologic impact to seawater circulation in near-shore aquifers.

Literature about density-driven flow in arid regions mainly focuses on interface characteristics within steady state hydrologic assumptions that ignore time-sensitive responses (Duffy & Al-Hassan, 1988; Ying Fan et al., 1996; Wooding et al., 1997). Due to limitations in analysis, studies that numerically assess saline intrusion usually examine a single changing influence on the interface's dynamics, such as changes in recharge [*Post et al.*, 2019] or discharge [*Werner and Simmons*, 2009]. However, most if not all of aquifers have multiple points of discharge and recharge that jointly impact an interface's response. Specifically for arid regions, basin-scale recharge trends can change over relatively short (i.e. interdecadal and millennial) timescales (Placzek et al., 2009) and hydraulics of shallow surface water bodies are particularly sensitive to changes in the groundwater table (Tyler et al., 2006). Therefore, shifts in precipitation rates can significantly impact both recharge and discharge to an aquifer. Regional aquifers may require millennia to respond to hydrologic changes [*Lu and Werner*, 2013; *Corenthal et al.*, 2016], highlighting the importance of considering climate change even if short-term hydrology appears to be stable (Zhu et al., 1998).

1.3.3 Hydrogeologic setting of salars

Salars often host brine-rich aquifers and consist of evaporites in basins in typically arid climates with an average negative hydrologic budget (Rosen, 1994). In salar environments, a negative hydrologic budget commonly results from high rates of evaporation that outpace recharge, which primarily comprises lateral subsurface inflow into the basin (Tyler et al., 2006). This imbalance results in the accumulation of evaporite minerals that develop over time into an extensive series of halite-dominant evaporite sequences, otherwise known as a halite nucleus (Eugster, 1980). Endorheic basins provide an ideal environment for evaporite accumulation due to their tendency to inhibit the effective discharge of incoming sources (Houston et al., 2011),

but salars also occur in open basins provided that a negative water budget exists (Rosen, 1994). Aquifers underlying salars are often located in arid regions that exhibit recharge-controlled water table configurations (Haitjema & Mitchell-Bruker, 2005) and thus rely on lateral subsurface inflow for recharge (Ye et al., 2016). As a result, such systems exhibit lateral groundwater flow as predicted by the Toth model (Carmona et al., 2000; Qureshi, 2011; Rissmann et al., 2015), which can include groundwater flow into a topographically defined basin from another basin (Y. Fan & Schaller, 2009; Maxey, 1968; Montgomery et al., 2003). While surficial recharge provides a mechanism for sustaining groundwater levels (Boutt et al., 2016a), lateral subsurface inflow represents a key recharge mechanism for aquifers adjacent to salars (Houston, 2009; Scanlon et al., 2006), which has been shown through numerical simulations of density-driven groundwater flow (Ye et al., 2016).

Convection of subsurface fluids is another phenomenon that occurs in brine-rich aquifers underlying salars (Duffy & Al-Hassan, 1988). Previous modeling confirms that density-dependent flow influences fluid convection (Ying Fan et al., 1996), and thus convection controls the dynamic response and migration of freshwater-to-brine interfaces in aquifers underlying salars (*Oliver*, 1992). While differences in density drive fluid convection, sediments need to have a permeability of approximately 10^{-14} m^2 or higher in order to permit significant convective flow (Wooding et al., 1997). Because evaporites commonly have low permeability characteristics that are too low for convection, their contact with higher-HK lithologies creates conduits for permeable pathways for groundwater flow within aquifers. Since the development of evaporite sequences requires specific climate and geochemical conditions, different salars may be at different stages along the continuum of evaporite accumulation (Figure 2). While mature salars

like SdA would exhibit a higher occurrence of permeable pathways, the degree to which hydrostratigraphic continuity impacts interface sensitivity remains uncertain.

The extent to which changes in discharge and recharge couple with the prevalence of permeable pathways to impact fluid convection therefore remains poorly constrained. Surface water bodies in salars represent an important component of an arid environment's hydrology because they provide critical points of discharge via evaporation (Jayne et al., 2016). Salars develop surface water bodies as a result of the hydraulic gradient producing groundwater discharge and surface water runoff (Anderson et al., 2002). For salars, surface water bodies are a source of high rates of evaporation because the surrounding evaporite sequences have low permeability and high albedo. The lack of solar radiation absorption due to high albeda prevents the transfer of heat energy which leads to evaporation, and thus evaporation in this area is limited to the lower albedo marginal zones (Vásquez et al., 2013). Evaporation from surface water bodies may also increase groundwater circulation (Ying Fan et al., 1996), though the evaporative effect of the surface water bodies may also inhibit brine-to-freshwater interface's sensitivity to changes in recharge (Wooding et al., 1997). The relationship between groundwater-to-surface water exchange and the sensitivity of brine-to-fresh water interfaces to migrate with changes in recharge thus requires further investigation.

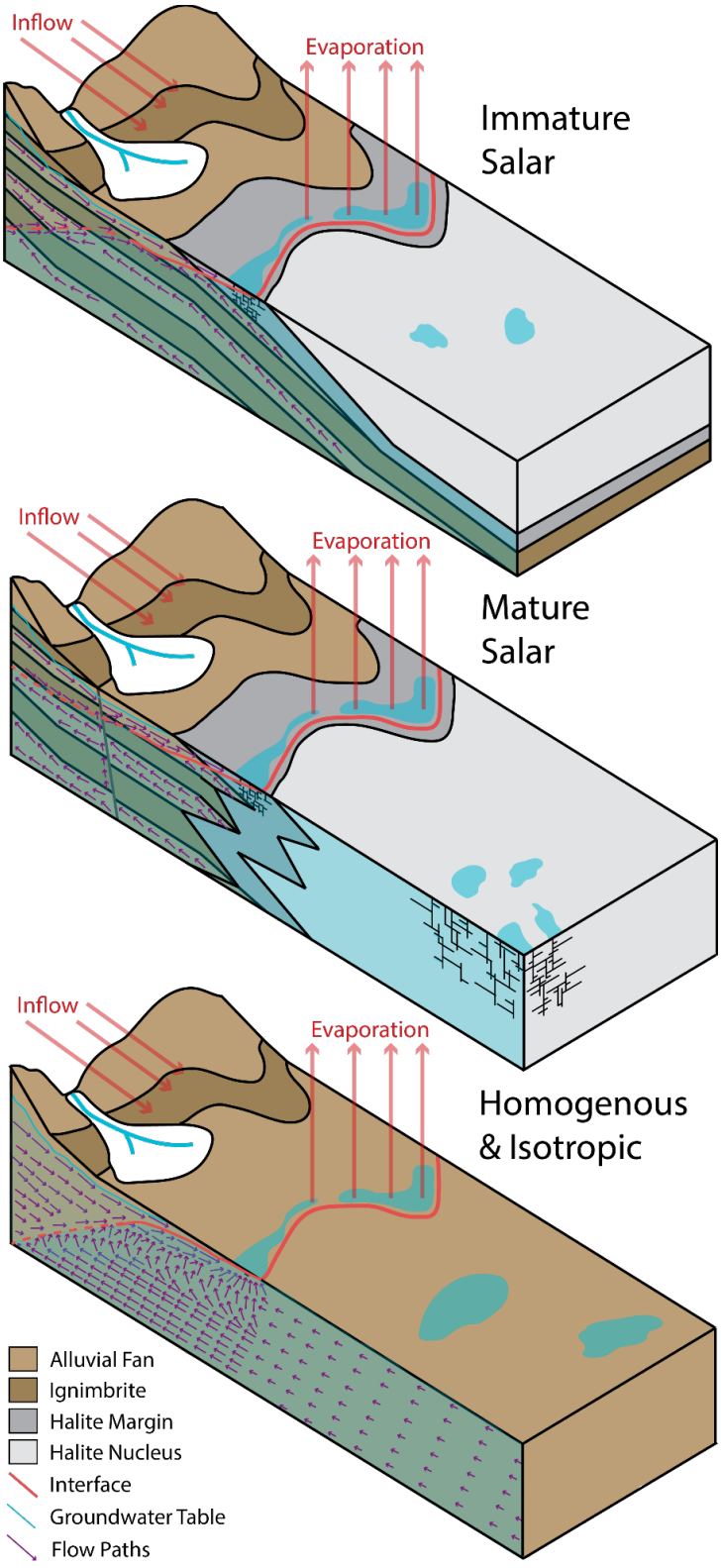

Figure 2 Conceptual illustration of mature versus immature salars ("salt flats") and their homogenous counterpart, with the resulting brine-to-freshwater interface and flow vectors.

1.3.4 Numerical simulation studies assessing density-driven flow

Numerical simulations of groundwater that account for density-driven flow primarily focus on coastal studies for the purpose of assessing the risk of seawater intrusion (Konikow et al., 2013; Liu et al., 2014; Morgan et al., 2012). There are a limited number of studies specific to arid, endorheic basins. They have primarily focused on density-driven groundwater circulation (Duffy & Al-Hassan, 1988; Ying Fan et al., 1996; Hamann et al., 2015). Studies have also documented the impact of evaporation (Tejeda et al., 2003; Tyler et al., 2006) and lateral subsurface inflow (Vásquez et al., 2013) on the steady-state impact on interface geometry. Marazuela et al. (2018) the first simulation results that document the shallowing of the interface with a lower-HK confining unit in arid basins (Figure 1). However, to date, there has been no study that has characterized the time-sensitive response of brine-to-freshwater interfaces to perturbations in subsurface lateral inflow.

1.4 Data sources and methods

Analyzing the role of stratigraphic continuity on interface sensitivity requires a parametric approach using a series of geostatistical realizations with a range of hydraulic conductivity values and distribution of lithologies documented in core data in SdA's southeastern margin (section S4). A separate hydrostratigraphic framework was developed for SdA's transition zone area, where brine interacts with inflowing freshwater along the southeastern area (Figure 21), in order to assess the site-specific implications for how subsurface heterogeneity impacts interface geometry and response to hydrologic changes. The hydrostratigraphic framework relies on a geologic model that was developed from core data, well data, surface geology, geophysical assessments, and knowledge of basin structure, which is further described in the supplementary sections.

1.4.1 SEAWAT simulations

Groundwater flow rates are assessed with variations in pressure gradients over distance using Darcy's Law for aquifers with a singular density. However, variable density aquifers require the inclusion of the density gradient coupled with solute transport in order to account for density's influence on groundwater flow movement (Langevin & Guo, 2006). Density-driven flow is accounted for by correcting the pressure gradient that determines fluid flow with equivalent freshwater head calculations for the degree to which density changes the pressure gradient (Post et al., 2007). A modified version of the Henry Problem serves as a semi-analytic solution for confirmation of simulation results (Langevin & Guo, 2006). Density-driven flow is simulated in this study using the above-described approach.

1.4.2 Initial & boundary conditions for model domain

The model domain and boundary conditions are based on representations of SdA's topography and presumed inflow and discharge conditions. As a parametric study, the distribution of the hydraulic conductivity is redistributed in a series of realization through a geostatistical Markov chain approach, as further described in section 1.4.3; other than the distribution of hydraulic conductivity, all other boundary and initial conditions remain the same, with exception of the sensitivity analysis of the subsurface lateral inflow rate. Figure 2 shows the model domain's geometry and initial and boundary conditions, with 100 m long by 10 m thick grid cells within the model dimensions of 13,000 km long by 300 m deep at its most topographically shallow point. The domain represents one side of a basin; the hypothetical symmetry of a basin renders the simulation of both sides unnecessary. The surface boundary is based on smoothed elevation models of the topography at SdA from the available 10 m-resolution digital elevation data. Specified head for the modeled edge of the nucleus on the left

side is set to 2299 masl, which is approximately 1 m below the modeled nucleus surface at 2300 masl. As seen in Figure 2, the entire left side of the model domain that represents the edge of the nucleus has a constant dissolved salt concentration of 200 kg•m^{-3}. The modeled subsurface laterally inflowing flux on the right side of the model domain has no concentration of dissolved salt. A head-dependent flux that equates to 0.7 mm•d^{-1} (i.e. a flux of 500 m^3•d^{-1} for the entire ET area) accounts for evapotranspiraition (ET) that occurs in the margin, which is determined based on evaporation estimates for SdA (Table 10). All other boundaries not otherwise described have no flux in either fluid or solute.

The initial solute concentration for the entire extent of the domain is 0 g•cm^{-3}. Initial hydraulic head is a uniform 1 m below the modeled surface. Respectively, values of longitudinal, horizontal transverse, and vertical transverse in all models are 10 m, 1 m, and 0.01 m. These values are consistent with modeling aquifers of this scale (Gelhar et al., 1992). Additional model conditions can be found in table 1. All iterations run with the above-described initial conditions to 3,000,000 days. The models then run for another 3,000,000 days following a perturbation in hydrologic conditions in order to assess the sensitivity of the interface.

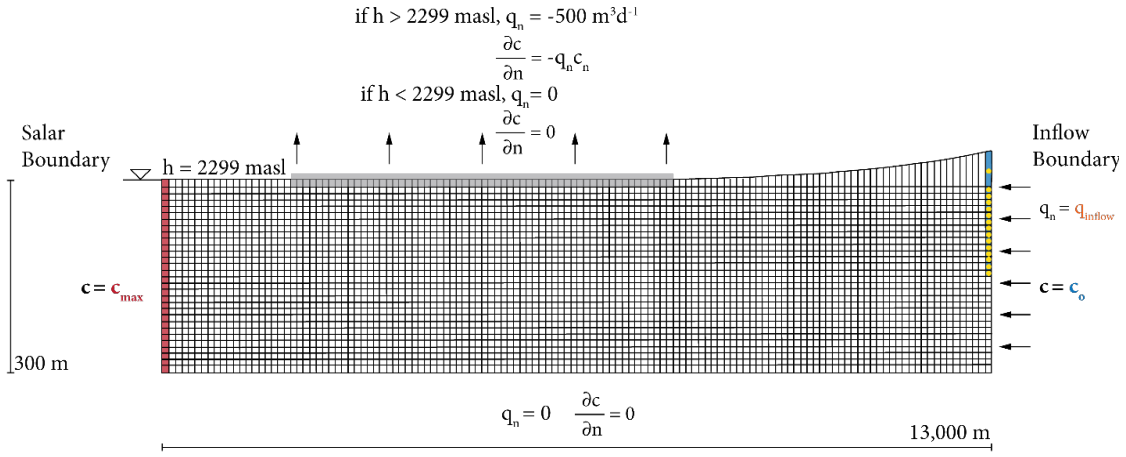

Figure 3 Boundary conditions for the 300 m deep by 13,000 m long 2-D model framework with a vertical exaggeration of 10. Note that the model is discretized into 30 by 130 cells each cell having the dimensions of 10 m

deep by 100 m wide. Also note that c_{max} = 200 g•L^{-1}, c_o = 0 g•L^{-1}, and that q_{inflow} varies by 300, 500, and 700 m^3•d^{-1}. Vertical exaggeration is 10.

Parameter	Value	Unit
Domain length	13,000	m
Domain thickness (B)	300	m
Longitudinal dispersivity (α_L)	10	m
Transverse dispersivity (α_L)	0.001	m
Diffusion coefficient	1•10^{-8}	m^2•s^{-1}
Effective porosity (ϑ)	0.3	-
Constant head at nucleus (h_n)	2299	masl
Freshwater density (ρ_o)	1,000	kg•m^{-3}
Brine density (ρ_{max})	1,200	kg•m^{-3}
Storativity (S_s)	1•10^{-5}	m^{-1}
Specific yield (S_y)	0.2	m
Vertical anisotropy of hydraulic conductivity	0.1	-

Table 1 Constant boundary conditions for the numerical modeling approach. These conditions are constant throughout the modeled time for every model. Note that the listed vertical anisotropy value applies for the non-isotropic models.

1.4.3 Changes in model parameters to simulate climatic change in recharge

Groundwater inflow is the only boundary in this study that experiences variation for the HSF, the homogenous model, and every realization of hydraulic conductivity. As listed in Table 1, all other parameters remain unchanged. The construction of these boundary conditions are based on assumptions of arid hydrology, as supported by site-specific data. Since arid basins exhibit minimal to no surficial recharge where ET outpaces precipitation rates (Scanlon et al., 2006), an important recharge mechanism of such basins is lateral groundwater flow following the Toth model (Y. Fan & Schaller, 2009). Thus, the impact of direct recharge is not considered. Table 2 shows the set of different hydrologic case scenarios that each model realization experiences.

Scenario #	Inflow (m^3•d^{-1})	Evapotranspiration (mm•d^{-1})
1	300	0.7
2	500	0.7
3	700	0.7

Table 2 The set of different inflow conditions to which each realization of the hydraulic conductivity distribution is exposed for sensitivity analysis. Evapotranspiration rates are per cell.

1.4.4 Changing distributions of hydraulic conductivity

A hydrostratigraphic framework (HSF) of SdA was developed by incorporating data from the study site's hydraulic testing into a geologic interpretation (S4). A homogenous model was also created and shares the HSF's effective conductivity (K_{eff}) of 10.3 $m \bullet d^{-1}$. K_{eff} was calculated using Darcy's law and simulated flux (q) values resulting from fixed hydraulic gradient numerical experiment. The geometry and dynamic response of the interface in both models were then compared to one another. This comparison was further informed by a series of simulations with equally probably distributions of hydraulic conductivity, as further described below.

Geostatistic realizations of heterogeneous distributions were based on hydraulic conductivity assigned to lithostratigraphic units from the study site in the southeastern margin of SdA. The hydraulic conductivity values are based on geologic and hydraulic data from the 32 cores and 27 wells from within the 17 km^2 that comprise the southeastern margin of SdA; the hydrostratigraphic interpretation is based on over 50 hydraulic tests that have occurred in the area. Each hydraulic test was assigned a lithostratigraphic facies based on the geologic unit in which the test occurred. As noted in table 3, the hydrostratigraphic interpretation were separated into five lithologic facies: medium-grain clastics from alluvial fan deposits (10 $m \bullet d^{-1}$), fine-grain carbonates (1 $m \bullet d^{-1}$), vuggy carbonates (100 $m \bullet d^{-1}$), un-fractured ignimbrite ($1 \bullet 10^{-1}$ $m \bullet d^{-1}$), and interbedded gypsum and carbonate ($1 \bullet 10^{-2}$ $m \bullet d^{-1}$). Values were stochastically determined within one standard deviation from the average of hydraulic conductivity for each of the facies. All realizations had the following proportions of lithologic facies: 43.1% fine carbonate, 23.5% alluvial fan deposits, 19% ignimbrite, 8.3% vuggy carbonate, and 6.1% gypsum carbonate mix.

The same overall proportions of hydraulic conductivity are then heterogeneously redistributed using a geostatistical approach. Three groups of realizations with distinct horizontal

to vertical stratigraphic continuity ratios were created to address the role of geologic complexity in the sensitivity of interface response: equal continuity in both directions, increase horizontal continuity by a factor of two, and increased horizontal continuity by a factor of three. Fifty 2-D realizations were created for each group of continuity ratios using Markov chain probability analysis, which is a common statistical approach for quantifying the probability of one condition transitioning to another, in the TPROGs software [*Carle*, 1999]. Only geostatistical realizations with K_{eff} values within ±10 $m \cdot d^{-1}$ of the original hydro stratigraphic framework's K_{eff} (10.3 $m \cdot d^{-1}$) were used in order to ensure comparable results.

The simulations were run to an initial steady state with no interface movement in order to establish an interface geometry from initial conditions. The initial steady state was determined based on the total mass of dissolved salt in the system. Assuming the response of salt mass follows an exponential rate of decay following a perturbation in the subsurface lateral inflow, the time constant that characterizes the exponential decay rate of change can be used to confirm the point at which salt mass is stable. After reaching an initial steady state, all realizations were subsequently exposed to the prescribed set of perturbations in inflow, as seen in Table 2.

In total, as listed in Table 4, the HSF, the homogenous model, and the 50 realizations from each group were simulated under the three different inflow conditions to create a total of 456 simulations. The geostatistical realizations along with the homogenous and the HSF model are then assessed using the same set of metrics, as described in section 1.4.5.

Lithostratigraphic Unit	**Assigned Hydraulic Conductivity ($m \cdot d^{-1}$)**	**Percent of Total Distribution**
Alluvial fan deposits	10	23.5
Fine-grain carbonate	1	43.1
Vuggy carbonate	100	8.3
Unfractured ignimbrite	0.1	19
Interbedded gypsum and carbonate	0.01	6.1

Table 3 Distribution and assigned hydraulic conductivity of each lithostratigraphic unit, which were used as the basis for the randomized distribution of hydraulic conductivity.

Model Type	# of Realizations	Total # of Simulations
Hydrostratigraphic framework	1	3
Homogenous model with K equal to Ke_{ff} of hydrostratigraphic framework	1	3
GR Group 1: Equal continuity in both the horizontal and vertical directions	50	150
GR Group 2: Increased continuity in the horizontal by a factor of one	50	150
GR Group 3: Increased continuity in the horizontal by a factor of two	50	150
Total	*152*	*456*

Table 4 The number of realizations and simulations in each model category for the study.

1.4.5 Metrics for assessing interface sensitivity & stability

Four metrics were used to assess differences in interface geometry, sensitivity, and stability among the 456 model iterations. The first and second metrics are the length of transition zone between fresh (i.e. < 40 g•L^{-1}) and highly saline (i.e. > 180 g•L^{-1}) groundwater [L] and the average slope of the interface, which was assessed with a linear best fit. These metrics were calculated to assess interface geometry. Third, the length of interface migration in the horizontal direction [L] provide a mean for assessing the sensitivity of the interface following a change in recharge to the modeled aquifer. Fourth, the time required for the interface to reach a new equilibrium following a perturbation to the system's hydrologic conditions [T]. The migration length is found by calculating the difference in the location of the 0.5 isoconcentration (i.e. 100 g•L^{-1}) point in the model domain following the perturbation of inflow into the modeled aquifer at $3 \cdot 10^6$ days. For the purpose of assessing stability, we use the response time required for an interface to restabilize following the perturbation of inflow. Stability is assessed via the accumulation of the total mass of solute in the model that exists in the system at any point in time, such that:

$$\int_{m_i}^{m_f} \frac{d_m}{d_t} = -k \frac{d_m}{d_t}$$

where k is the rate at which the mass of dissolved salt in the system reaches a statistically insignificant rate of change. Assuming that the rate of change is an expression of exponential decay following a perturbation, the rate then fits an exponential curve such that:

$$\frac{[m]_f}{[m]_i} = e^{-kt}$$

where the ratio of the change in mass is equal to the rate of change over time. We therefore use the exponential time constant, amount of time required for the rate to change by a factor of *e* (i.e. "e-folding time") as the metric for comparing stability across all models. For the purpose of this study, the e-folding time serves as a characteristic of the response rate, with the time corresponding to the speed of response to reaching a new steady state.

1.5 Results: Observations from results of numerical simulations on the geometry and dynamics of brine-to-freshwater interfaces

1.5.1 Geometry & dynamic response of the hydrostratigraphic framework of Salar de Atacama

Figure 5 shows the solute concentration values, head gradient, and velocity field of the homogenous model that represents the bulk K_{eff} of the HSF of SdA. Solute concentration values show an even transition zone from 0 to 200 g•L^{-1} with depth, though the upper 50 meters of the model near the area of modeled evaporation appears to have a wider transition zone. The head gradients and flow velocity field reflect the geometry of concentration values, with higher head values at depth in the saline fluid forcing fluid convection and upwelling. The homogenous model's concentration values diverge from observed field conditions (Figure 4).

Compared to its homogenous counterpart, the heterogeneous model that represents the hydrostratigraphic framework of SdA is shallower, more sensitive to changes in subsurface lateral inflow, and is also more unstable to those changes in terms of the time required to cease interface migration. Numerical results shown in Figure 3 indicate that the geometry of the

interface, as represented by the location of the 0.5 isoconcentration line through the model domain, show a distinctly shallower geometry, especially towards the upper 100 meters of the model. Figure 7 shows the e-folding time to reach a new steady state in response to inflow perturbations is larger by at least a factor of three for the HSF model when compared to the homogenous model. The total distance that the interface travels as a result of a change in inflow, as assessed through the movement of the 0.5 isoconcentration line, likewise exhibits a distinct difference between the heterogeneous and homogenous models, with interface travel through permeable pathways within the heterogeneous model.

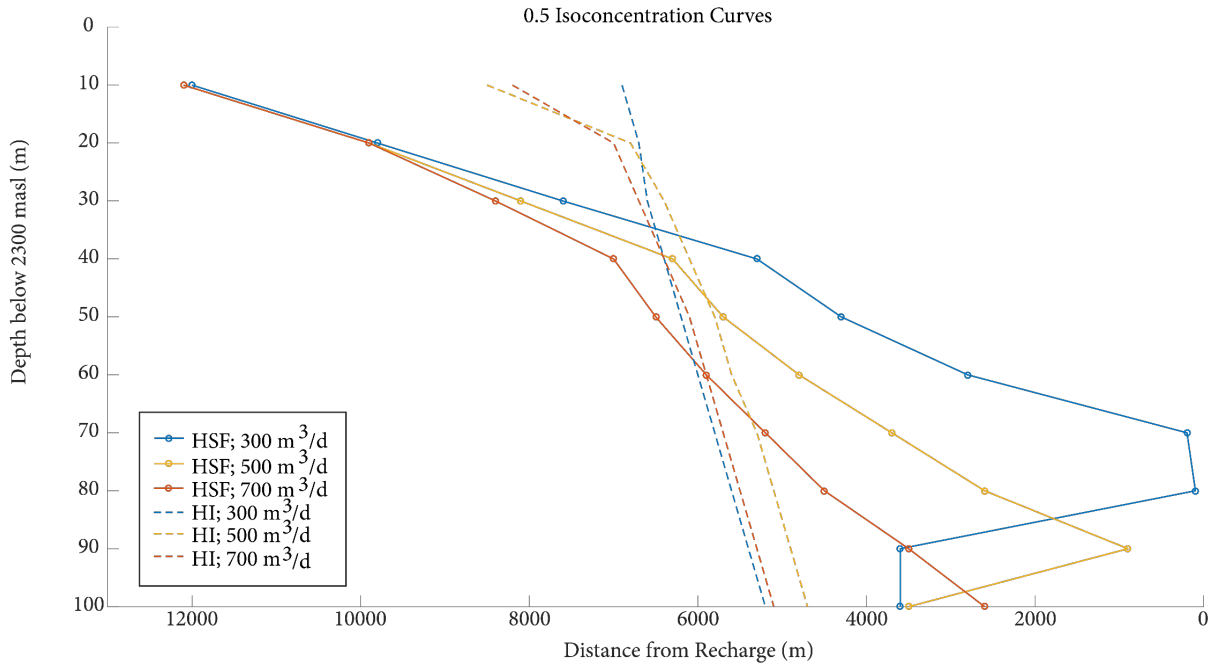

Figure 4 Modeled simulation results of the location of the 0.5 isoconcentration curve (100 g/L) for both the heterogeneous model of the hydrostratigraphic framework (HSF) and the homogenous (HI) model. Blue indicates the location after a decrease in inflow, red is the curve following an increase in inflow, yellow is no change in inflow.

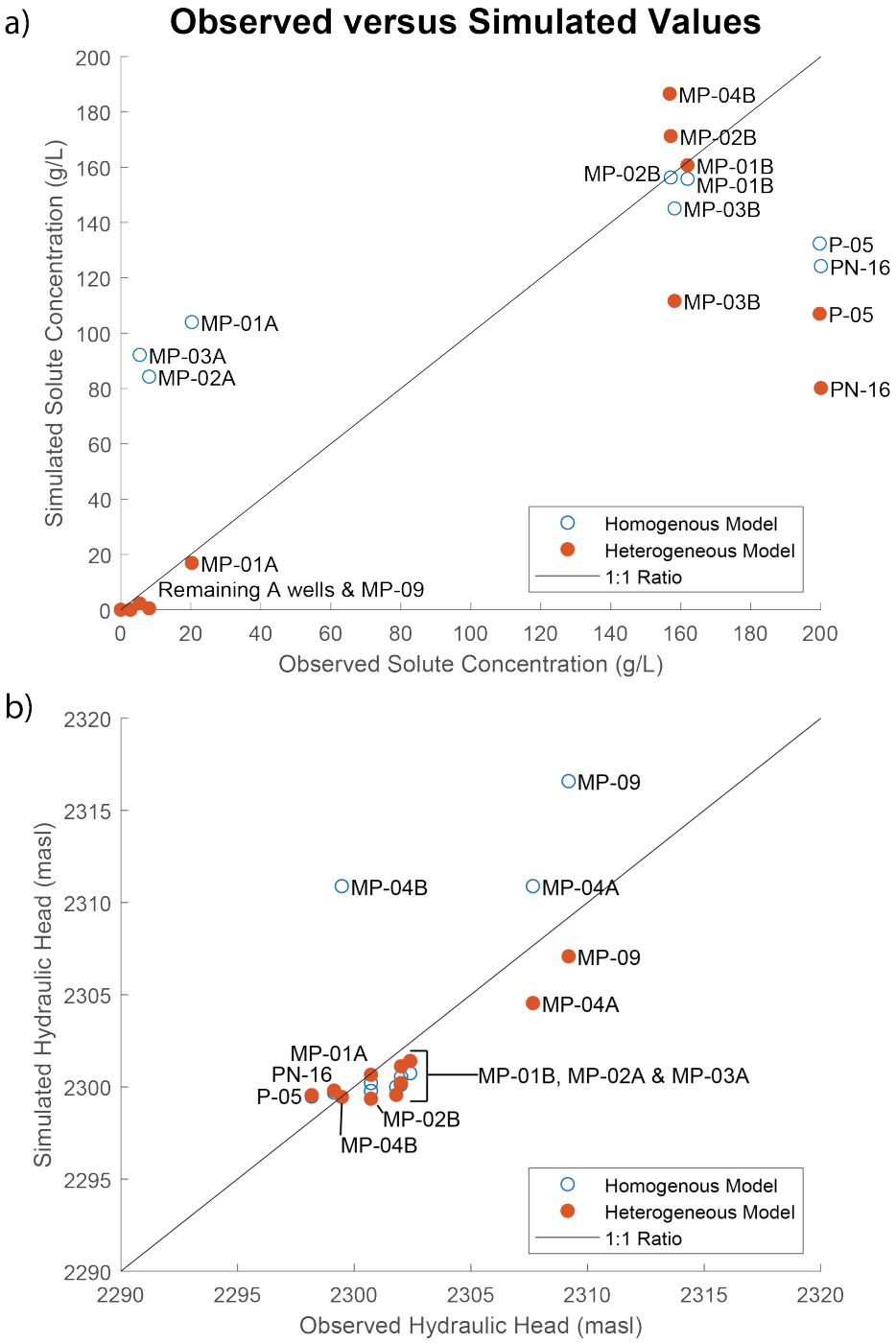

Figure 5 Observed versus simulated values for both a) the concentration and b) the head for the homogenous model (open blue) and the heterogeneous model based on the hydrostratigraphic framework (closed red). RMSE for concentration values are 48.87 for the heterogeneous model and 70.97 for the homogenous model, and for head are 1.6 for the heterogeneous model and 4.37 for its homogenous counterpart.

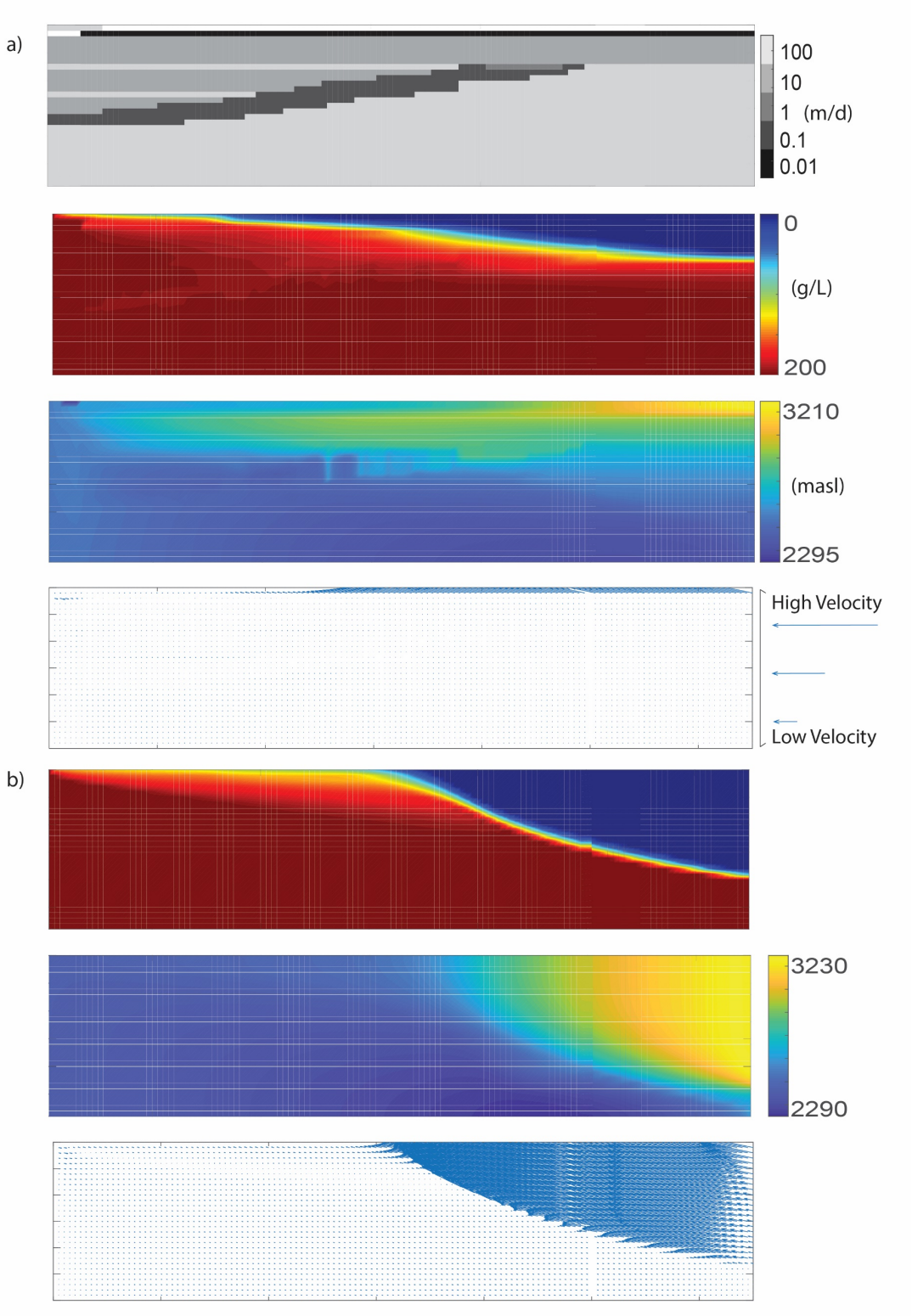

Figure 6 Visual comparison of the distribution of concentration (g/L) of dissolved salt in the modeled aquifer, the hydraulic head, and the velocity vectors for both the a) heterogeneous model based on the hydrostratigraphic framework and b) the homogenous model with the same K_{eff}.

1.5.2 Geometry & dynamic response of geostatistical realizations to changes in inflow

Simulations with equally probable distributions of hydraulic conductivity produce results that diverge from their homogenous counterparts and show a strong relationship with stratigraphic continuity in a geologically complex environment. The simulations show interface geometries that decrease in slope as hydrostratigraphic continuity increases in the horizontal direction. The range of locations for the interface for each group of geostatistic realizations is shown in Figure 8. Homogenous models with equivalent K_{eff} as the realizations produce interface geometries that are steeper by at least a factor of two and in some cases by an order of magnitude (Figure 6). The average slope for each group of realizations increases by a factor of one for every increase in the ratio of horizontal to vertical hydrostratigraphic continuity by a factor of one. Similarly, the thickness of the transition zone between saline and freshwater also shows a pattern of generally decreasing while expressing more variation in diffuse versus sharp concentration gradients as horizontal continuity increases, whereas the homogenous models show a consistently thicker transition zone (Figure 9).

The response of interfaces in the geostatistical realizations follows a statistically significant pattern for both the sensitivity and stability of the interfaces. Increased horizontal continuity of hydrostratigraphic units in the realizations yields an increase in the overall length of interface migration and thus presumably creates an increase in the sensitivity of density-driven flow to changes in subsurface later inflow into an aquifer. Similarly, an increase in the horizontal continuity results in longer time constants in the exponential decay of an interface's migration rate (Figure 7). From least to most continuous, the geostatistical realizations respectively yielded average interface migration of 651 ± 254 km, 967 ± 968 km, and 1270± 922 km. This equals an increase of 48% and 31% in average migration for each respective increase in horizontal

continuity by a factor. For the exponential decay in the interface response, the average time constant was 2830 yr, 6566 yr, and 9793 yr for each group from least to most continuous, creating a 230 % and 150 % increase in time for each respective increase in continuity. These observations are statistically significant to a 98% confidence level, except for three simulations for the average length of migration and five simulations for the exponential time constant. Comparatively, the brine-to-freshwater interface migration within the homogenous models exhibit significantly less sensitivity in terms of the amount of interface movement and more stability in terms of a decreased time required to reach a new steady state subsequent to being exposed to the same perturbations in subsurface lateral inflow.

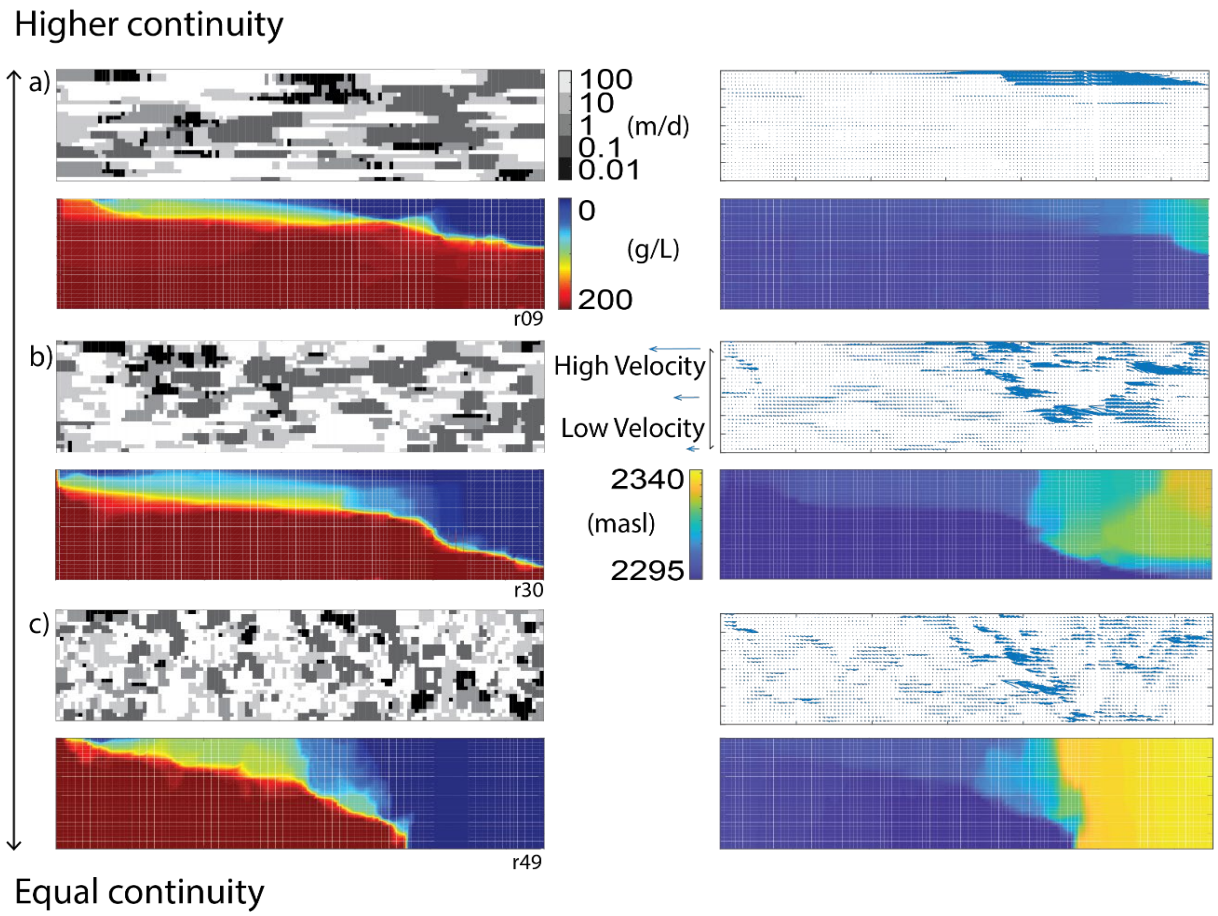

Figure 7 Visual comparison for one example in each group of geostatistical realizations, with a) increased horizontal hydrostratigraphic continuity by a factor of three at the top, b) increased horizontal hydrostratigraphic continuity by a factor of two, and c) equal continuity in both the horizontal and vertical directions. For each group,

in the upper left corner, the example model's distribution is shown in m/d. The upper right for each group is the distribution and direction of groundwater flow velocity vectors, with arrow sizes proportional by an order of magnitude to the velocity rate. The lower left is the model results for the distribution of concentration (g/L) of dissolved salt in the modeled aquifer. The lower right in reach group is the distribution of hydraulic head values.

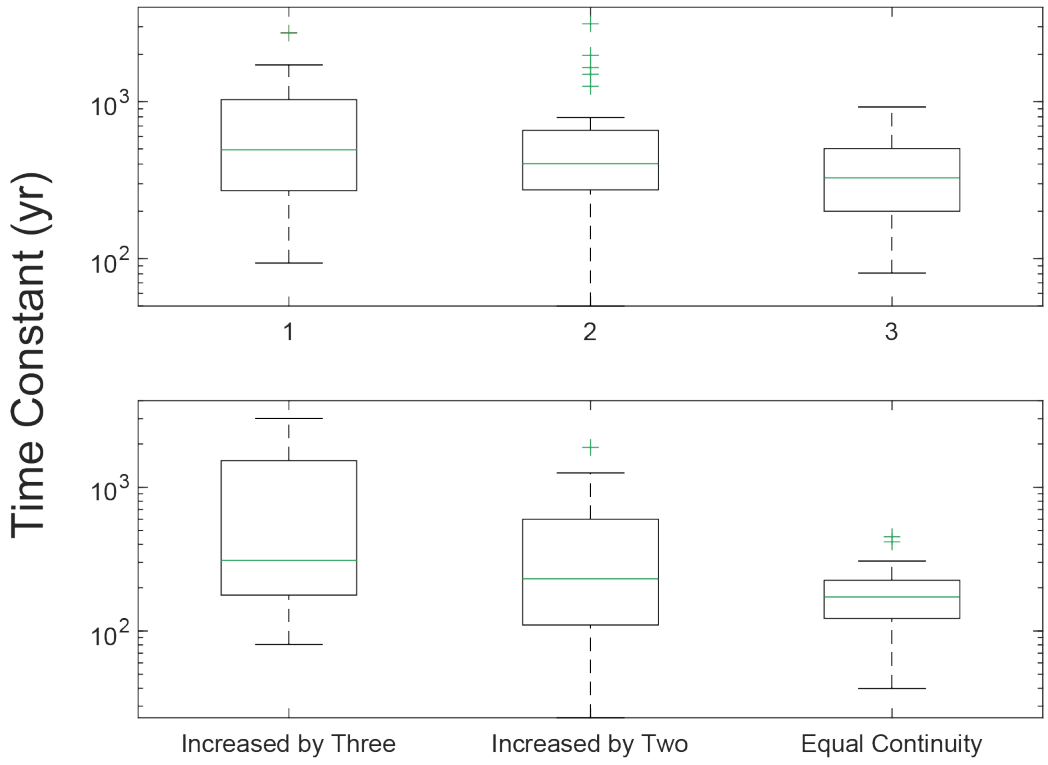

Figure 8 The distribution of time constant values representing the exponential decay rate that each realization of hydraulic conductivity distributions experiences following a perturbation of inflow. Results are separated by both ratio of horizontal continuity to vertical continuity and by type of perturbation (increasing versus decreasing in inflow).

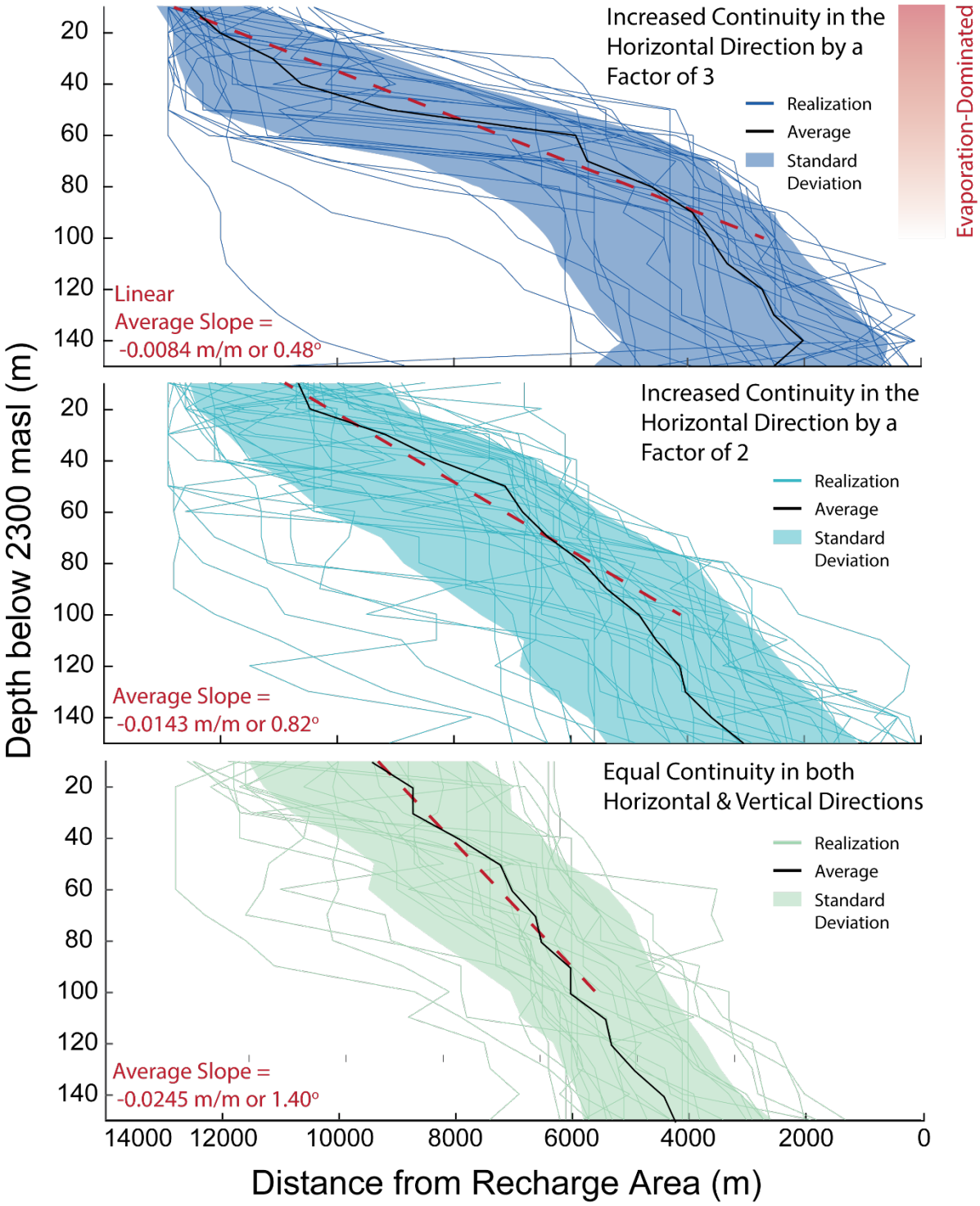

Figure 9 Distance of the 0.5 concentration point from the recharge area with depth for each group of geostatistical of hydraulic conductivity. Each group of realizations is separated based on degree of continuity, with increased horizontal continuity by a factor of three (dark blue), increased horizontal continuity by two (light blue), and equal continuity (green) in order from top to bottom. The value for the linear best fit (dashed red) for the median (solid black) of each group is listed in the lower right corner of the graphs. The shaded region is the standard deviation.

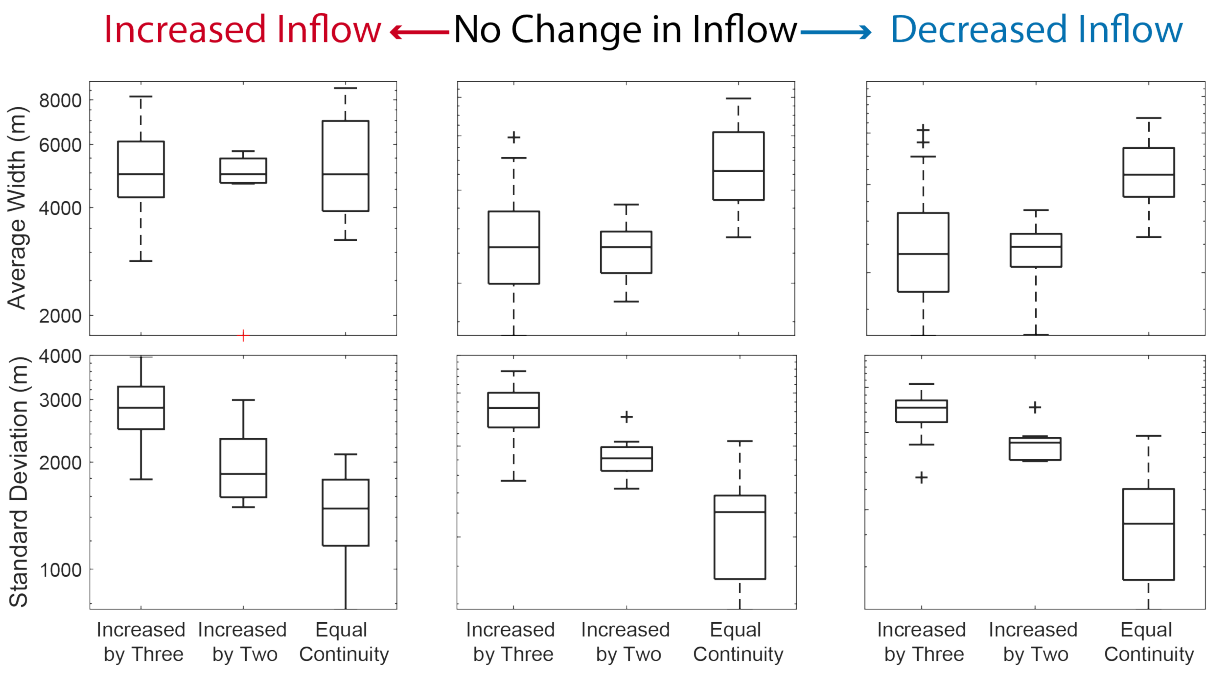

Figure 10 The distribution of average transition zone widths from freshwater (40 g/L) to brine (180 g/L) for the geostatistical realizations of hydraulic conductivity, separated based on horizontal hydrostratigraphic continuity as compared to vertical continuity.

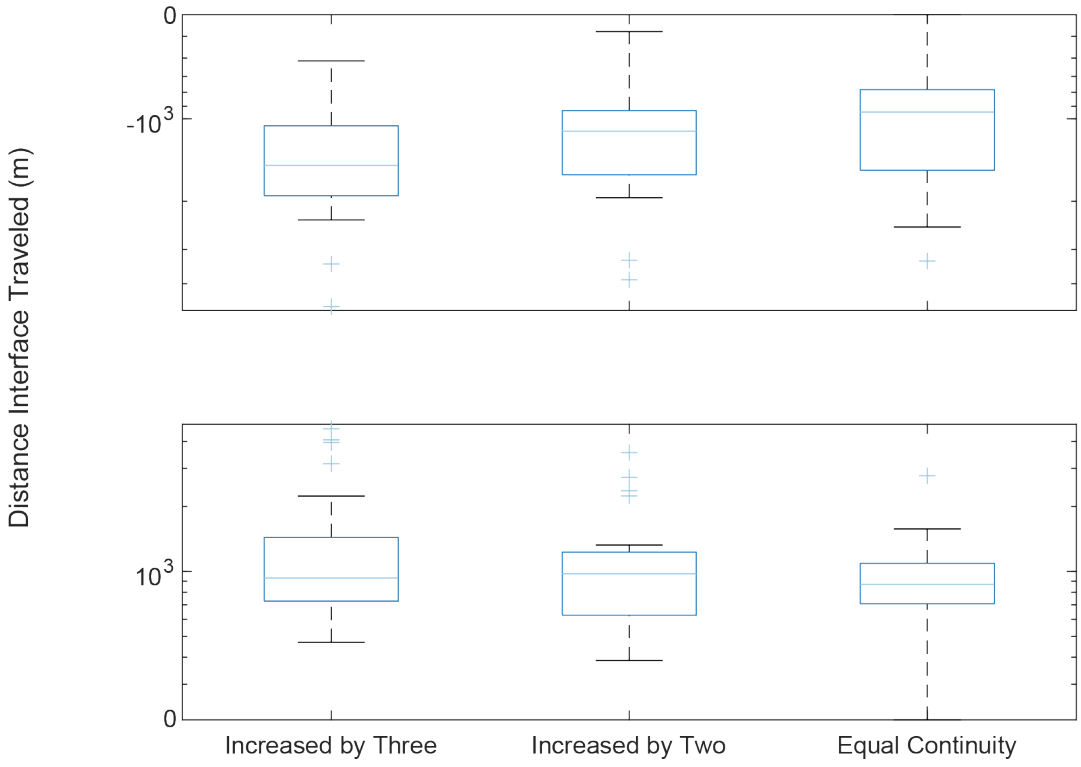

Figure 11 Distribution of average distance traveled based on the movement of the 0.5 isoconcentration line after the perturbation of inflow. The upper boxplot is an increase in inflow and the lower box is a decrease in inflow. The

simulation results are separated based on the amount of horizontal hydrostratigraphic continuity as compared to vertical continuity.

1.6 Discussion

1.6.1 Interface sensitivity to changes in inflow

Regardless of modeled hydrogeologic conditions, brine-to-freshwater interfaces in salar environments respond to changes in inflow. An increase in inflow rate forces the salar-ward migration of the interface; a decrease in inflow likewise causes the opposite effect with a recharge-ward migration of the interface. This general response is consistent with previous density-driven interface modeling (Liu et al., 2014; Y. Yechieli et al., 2001; Yoseph Yechieli, 2000). Due to the boundary conditions of the simulations, the interface's response to an increase in inflow is generally less in terms of length in migration and time to reach equilibrium as compared to decrease in inflow. This characteristic is an expression of the constant concentration boundary condition of the model, as illustrated on the left side of the 2-D framework in Figure 2, where the concentration is fixed on the salar-ward side of the model. The fixed concentration of the salar boundary maintains a density gradient despite changes in simulated laterally inflowing freshwater from the right side of the model. While this response technically represents the limitations of the model's boundaries, it also confirms that the location and thickness of SdA's halite nucleus exerts primary control in the geometry of the interface and sensitivity of the interface migration to changes in subsurface lateral inflow. The halite nucleus as a constant source of solute provides a stabilizing effect in terms of the interface's reaction to hydrologic conditions that could potentially drive a salar-ward migration.

Considering that recharge is likely to decrease in arid climates as a result of climate change, it is prudent to focus on the impacts of decreased inflow in the models. Modeling suggests that interfaces migration distances are between 10-35% more sensitive to a decrease

than an increase in inflow. These reactions highlight the importance of accounting for changes in inflow into an arid basin specifically.

This modeling study does not incorporate gradual changes in inflow and therefore the applicability of interpreting the interface's response may be limited in terms of modeling realistic conditions. Considering that fluctuations are common aspects to hydrologic conditions in environments that host saline aquifers, this is a recognized gap of knowledge in the understanding of interface dynamics and therefore merits further investigation.

1.6.2 Impact of increased stratigraphic continuity on interface sensitivity and stability

Varying horizontal continuity in hydrostratigraphic units for geostatistical realizations of hydraulic conductivity provides a method for assessing the effects of geologic complexity and lateral continuity on a brine-to-freshwater interface's sensitivity to changes in recharge. Comparing the results of the hydrostratigraphic framework model versus the homogenous model, the interface resulting from the heterogeneous model based on the hydrostratigraphic interpretation exhibited an increased migration distance and a longer response time to reach a new steady state than its homogenous counterpart. This comparison suggests that horizontal continuity controls both the sensitivity and stability in the dynamics of an interface in response to changes in recharge. Results from the geostatistical realizations further indicate that an increase in the continuity of hydrostratigraphic units leads to a longer exponential decay constant that represents the time required for the modeled aquifer to reach a new steady state following a change in subsurface lateral inflow. Based on the geostatistical realizations, increased continuity in the horizontal direction further indicates that an interface's dynamics are more sensitive to a perturbation in the aquifer's inflow based on the length an interface travels following a change in inflow. An increase in the continuity of hydrostratigraphic units leads to an increase in the

prevalence of highly conductive preferential pathways and thus increases the potential for instability with longer time required for the interface to reach a new stable position and sensitivity in terms of length of interface migration in response to changes in recharge to the aquifer.

Results for the response time required to reach a new steady state are given as a time constant in order to provide a relatable metric for all models. The time constant values produced from the geostatistical realizations of hydraulic conductivity distributions may not be directly comparable to in situ conditions because the models do not capture realistic expressions of subsurface hydrogeology. Therefore, analysis of these time constant values is limited to comparison among models. While a simple comparison with the HSF model indicates that most of the time constant values may seem plausible for playa environments, the question of the realizations' geologic plausibility impedes the ability to rely on time constant values produced from these models as realistic scenarios. However, it is possible to assess stability in comparative terms among the groups of geostatistical realizations, as listed in Table 5.

Results indicate that the response rate required to reach a new steady state varied in a direct relationship with effective hydraulic conductivity (K_{eff}). Figure 11 shows that the K_{eff} versus the time required to reach equilibrium have a direct relationship, suggesting that the overall connectivity of an aquifer's hydostratigraphic framework also impacts the brine-to-freshwater interface's dynamic response to hydrologic changes in the aquifer. Previous studies have clearly established this direct relationship and its expression in these simulations therefore reaffirms accepted empirical evidence.

While K_{eff} shows a relationship with stability, results from the numerical simulations of the equally probably distributions of distributed hydraulic conductivity values also maintain a

dependence to continuity irrespective of K_{eff}. Figure 11 shows the distribution of K_{eff} for the geostatistical realizations grouped according to degree of continuity in hydrostratigraphic units and indicates similar K_{eff} values for the model. While this relationship indicates that continuity impacts interface dynamics as a result of changing K_{eff}. However, the variety in the K_{eff} values suggests that applying K_{eff} cannot reliably predict interface response to perturbations in subsurface lateral inflow. If a hydrostratigraphic unit with higher HK is more continuous in the horizontal direction than the vertical direction, it is more likely to control K_{eff} in the horizontal direction. It is therefore critical to consider the role of continuity when assessing modeled interface's geometry and sensitivity.

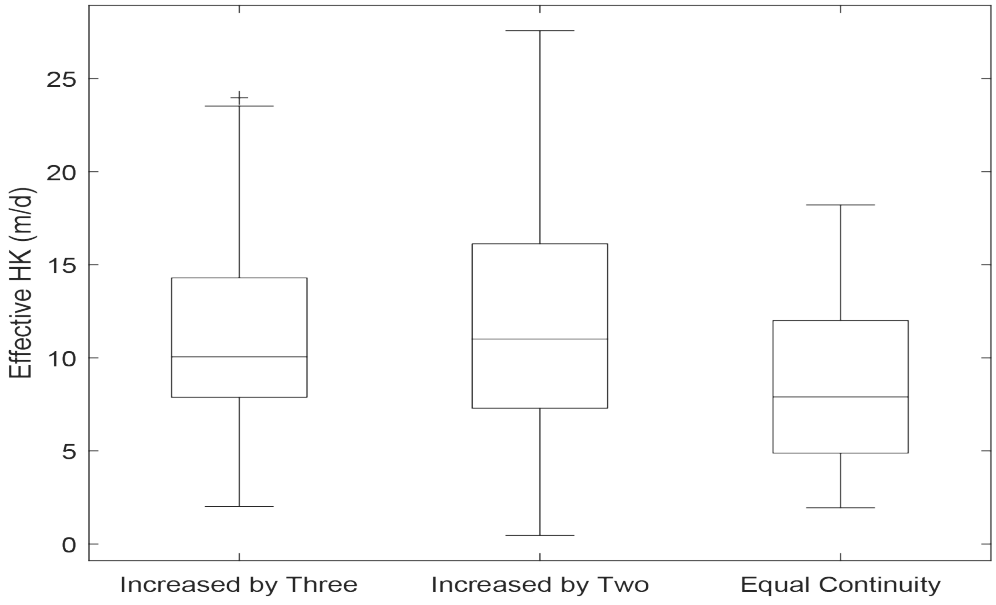

Figure 12 Effective hydraulic conductivity for numerical simulations separated by amount of horizontal continuity.

Group	Average Time Constant (yr)	Percent Difference from Homogenous Model
Equal Horizontal Continuity	262	5
Double Horizontal Continuity	960	23
Triple Horizontal Continuity	1281	43

Table 5 Average time constant comparisons among models between geostatistic realizations of hydraulic conductivity and their homogenous counterpart (i.e. equal K_{eff}), and the percent difference between them. (Note: These values are subject to change.)

1.6.3 Interpreted impact of modeled ET to interpretations of interface sensitivity

Since ET remained constant throughout the modeling, an analysis of impact of changing ET on the brine-to-freshwater interface sensitivity is beyond the scope of this thesis. However, it is possible to infer the potential impacts from ET on the interface based the sensitivity analysis of the simulation results. In particular, a remarkably consistent characteristic of the simulations' response to changes in inflow was the relatively unchanged area of ET, based on the location of cells in the top row of the model where ET occurred. When the interface's confluence with the surface intersected the ET area, the interface's migration distance in response to perturbations in the aquifer's inflow was usually lesser by an order of magnitude compared to the average length of migration of the cells at depth. This ubiquitous observation confirms the importance of considering potential ET in arid aquifers with abundant brine.

1.6.4 Implications for predicting the risk of saline intrusion in arid basins

Increased horizontal hydrostratigraphic continuity creates brine-to-freshwater interface dynamics that differ from predictions based on homogenous numerical models of density-driven dynamics of fluid flow. Results from the geostatistical realizations of hydraulic conductivity distributions show a direct relationship between lateral hydrostratigraphic continuity and interface geometry with little or no change in K_{eff}. Based on these results, geologic heterogeneity and hydrostratigraphic continuity are controlling factors in an interface geometry. This is especially critical for arid basins, where the development of transitional evaporite facies creates locally continuous units. In salt flat environments, the prevalence of strictly continuous boundaries of evaporite series against higher-permeability facies may account for the shallowing behavior of observed interfaces. As a result, aquifers with continuous stratigraphic contacts between high and low permeability units may develop distinctly shallower interface geometries

than traditional homogenous or simplistic models, where higher-K units act as conduits for fluid flow. This is especially true for transitional and depositional environments such as coastal environments and arid endorheic basins.

The trend of an increasingly shallowing interface with increasing horizontal continuity is likely more prevalent in arid basins with high rates of ET. Hydraulic head gradients redistribute closer to the surface in order to account for water loss via ET, which results in upwelling of groundwater. Brine-to-freshwater interfaces may thus appear to further shallow where the location and distribution of ET coincides with the interface's confluence with the surface. This evaporation-dominant pattern occurs through the upper 50 meters in all simulations in this study. However, due to more vertically conductive flow, the homogenous models tend to exhibit less apparent expressions. While ET clearly impacts interface geometry to a degree, the extent to which ET controls interface geometry and dynamics when coupled with geologic heterogeneity and recharge requires further sensitivity analysis.

Results further suggest that beyond the geometry of interfaces, hydrostratigraphic continuity also impacts the response of the interface to possible climate-driven changes to an arid aquifer's recharge mechanisms. Results from the geostatistical realizations indicate a statistically significant increase in sensitivity of the brine-to-freshwater interface to changes in subsurface lateral inflow and decrease in the stability of the interface as hydrostratigraphic continuity increases. In some cases, the increase in interface migration is over an order of magnitude higher with an increase in the continuity by a factor of two. The impact of lateral hydrostratigraphic continuity on the response of interfaces relates to an aquifer's lack of connectivity creating a unstable hydraulic field. Longer, high-permeability conduits result in local preferential pathways with hydraulic conditions that may differ from the bulk hydraulic conductivity. These pathways

create smaller-scale confining conditions within an aquifer that decrease the stability of the aquifer as a whole by creating in a lag in response time and thus increasing the total time required for an interface to cease migration. Since high horizontal continuity is a common feature in geologically depositional environments, such as salt flats specifically, and arid, endorheic basins in general, homogenous or simplistic modeling methods underestimate both the total amount of possible saline intrusion and the timescale at which migration can occur. The impact of hydrostratigraphic continuity on density-driven responses to hydrologic perturbations therefore needs to be addressed in such environments in order to produce more accurate predictions to climate-driven saline intrusion.

1.6.5 Implications for future modeling of density-driven flow in arid basins

Current density-driven modeling of arid, endorheic basins typically produce simple representations of an aquifer, using homogenous changes in anisotropy or simple layers with differing hydraulic conductivity values in order to shallow the interface geometry and match model results with observed field conditions. Without considering the geologic complexity or continuity of hydrostratigraphic units in an aquifer, such models result in conditions that may not produce either accurate geometries or reliable saline intrusion predictions. While simple changes in anisotropy may produce interface slopes that approach observed conditions, they do not account for local variation in the geometry, including the observed shallowing trend seen in the upper 50 meters of the aquifer of SdA. This sensitivity analysis documents that this shallowing trend impacts the density-driven response to changes in inflow. Accurate estimations of saline intrusion therefore require precise modeling of an aquifer's geologic complexity in order to more effective assess geometry as well as response to changes in an aquifer's recharge and discharge mechanisms.

Geostatistical realizations of hydraulic conductivity distribution provide an option for assessing density-driven flow in aquifers where significant geological data gaps exist. While it is usually impossible to gather sufficient data to fully characterize the hydrostratigraphic conditions of an entire aquifer, methods for assessing an aquifer's risk to saline intrusion can address gaps of knowledge. Rather than providing a simple range of predictions based on one or several hydrogeologic interpretations, including a geostatistical assessment of available hydrogeologic data represents a robust attempt to constrain a range of possible saline intrusion estimations.

1.6.6 Gaps of knowledge in the current modeling approach

It is recognized that geostatistically generated simulations may not be exactly representative of depositional environments of salt flats. Evaporite sequences produce geochemically zoned areas that often abut facies with distinctly different hydrogeologic characteristics. This creates an asymmetric distribution of hydraulic conductivities, which are not captured in this current geostatistical approach. Thus randomized distributions of hydraulic conductivity do not accurately represent geochemical zoning that occur in salt flats, and this study does not address the non-random horizontal as well as vertical changes in hydraulic conductivity that occurs in such transitional environments. While this parametric modeling analysis focuses on role of continuity rather than attempting to imitate real conditions, the lack of accurately representing geologic conditions in these realizations is recognized as a gap of knowledge. Future attempts to further constrain density-driven flow dynamics in such environments could develop semi-random distributions of hydraulic conductivity, in which lower-permeability units remain constant through each realization.

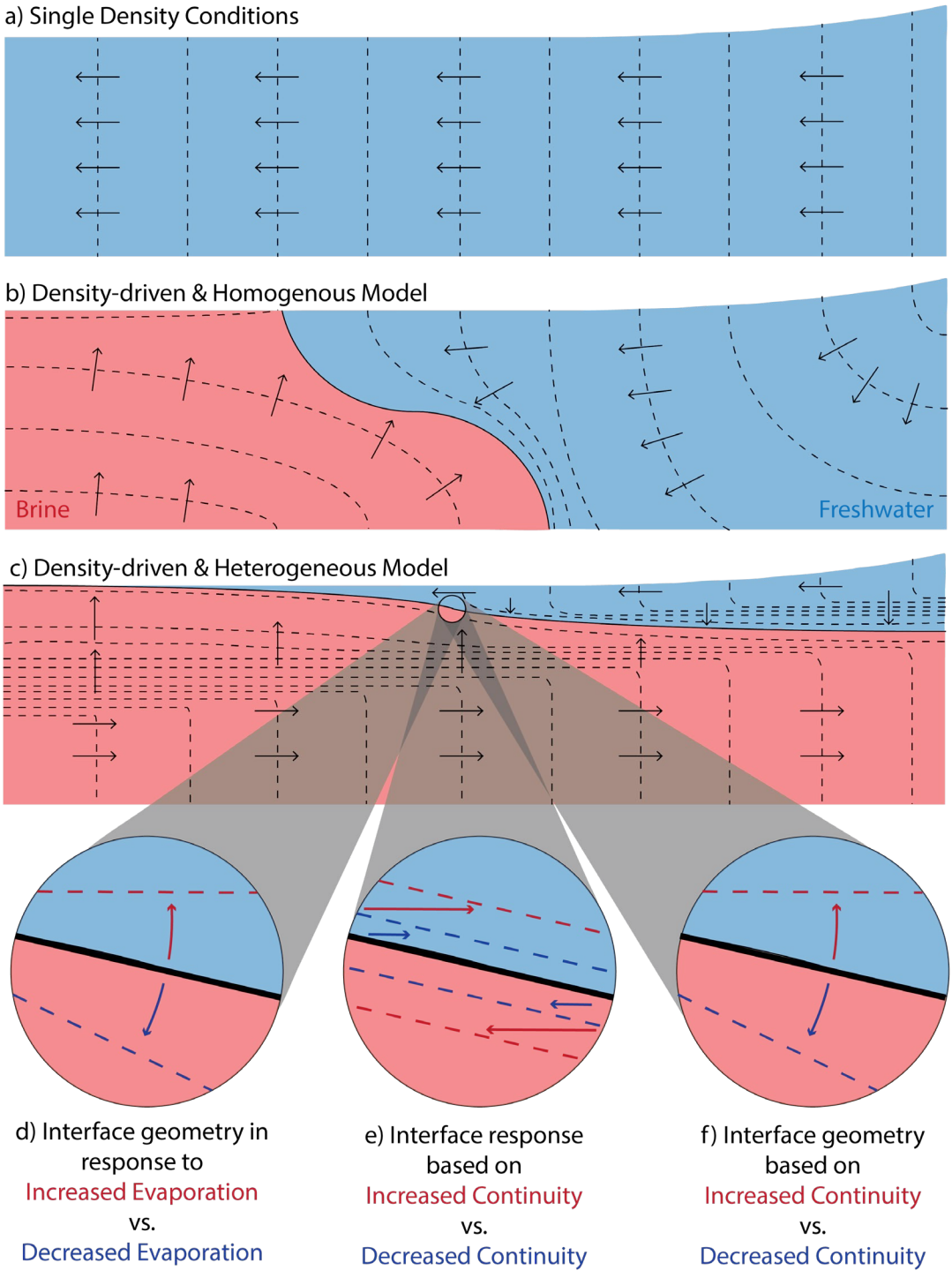

Figure 13 Conceptual illustration of results from observations of simulations with different distributions of hydraulic conductivity, with a) A homogenous, single-density flow with black dashed lines showing potentiometric head contours, b) a homogenous, variable-density flow model where the main determinant of interface geometry is the difference in density, and c) a heterogeneous model where the geometry of the interface is dependent on density, d) the extent and rate of evaporation, and f) the degree of continuity among hydrostratigraphic units. Continuity also controls the sensitivity and stability of the interface as well (e).

1.6.7 Applicability of modeled interface conditions to other aquifers

While the modeled hydrostratigraphic framework (HSF) produces results that match observed conditions for the available data points in SdA, the geostatistical realizations of the HSF's hydraulic conductivity distributions may indicate the degree to which observations of the interface's behavior can extend to other interfaces in differing hydrogeologic conditions. In this case, the specific hydrogeologic condition is the impact of continuity in hydrostratigraphic units. By using the same proportions of hydraulic conductivity from the hydrostratigraphy and randomizing its distribution, the geostatistical realizations can depict statistically equal hydrostratigraphic scenarios while varying the likelihood of horizontal continuity. While the realizations may not produce geologically realistic scenarios, statistically random realizations generalize the conditions observed at SdA and provide observations on the geometry and the movement of interfaces given such generalized conditions. The use of geostatistics is further supported by the stratigraphically complex nature of transitional and interbedding evaporite sequences, which are further complicated by a spatially variable structural regime that reflects SdA's diverse tectonic history. Therefore, the use of geostatistics expands the interpretation of interface geometry and sensitivity in endorheic, arid basins specifically, though interpretation can also expand to other environments with complex stratigraphic and tectonics regimes.

Changing the probability of hydrostratigraphic continuity in the horizontal direction addresses the question of geologic impact on both interface geometry and sensitivity. Increased continuity in hydrostratigraphic units increases the likelihood of modeling geologically realistic conditions in a depositional evaporite environment. A comparison of different degrees of hydrostratrigraphic continuity therefore provides an assessment of possible geologic impacts, as modeled through differences in hydraulic conductivity, on the dynamics of interfaces.

Comparing statistically significant numbers of models with similar ratios of continuity in the horizontal versus the vertical dimension allows for a more generalized interpretation of geologic impact on interface dynamics.

1.6.8 Limitations of model's boundary and initial conditions on sensitivity analysis

The construction of the model has several recognized limitations in terms of its applicability to real conditions. One recognized limitation is that several hydrogeologic conditions remain homogenous throughout the model's extent despite their direct correlation to changes in hydraulic conductivity. These conditions that would be intrinsically heterogeneous yet remain homogenous include specific yield, porosity, and anisotropy. While these characteristics all hold a positive relationship with hydraulic conductivity (HK) and would increase as HK increases, they remain consistently homogenous for computational simplicity given the number of geostatistical realizations in the scope of this modeling approach. However, it is recognized that constant and homogenous values for these variables impact the models' results by not accurately representing the full impact of variations in the hydrostratigraphy. As a result, because of these homogenized conditions, the dynamic response of the interface may not be fully expressed within the model's capacity. Future work in interface sensitivity would therefore benefit in an exploration of incorporating variations in these properties.

1.6.9 Limitations on the use of geostatistical realizations

The development and application of geostatistical realizations has several limitations that may impact the interpretation of the above-described model results. A primary concern is that the data gaps in the hydrostratigraphic framework discussed in section 1.5.4 cannot constrain the spatial relationships of the transitional facies among the lithologies and therefore introduces uncertainty into the analysis. The geologic conceptual model aims to address this known

unknown with geologically reasonable interpretations; however, the exact distribution of hydraulic conductivity based on the geologic conceptualization only transfers to the model that represents SdA and does not represent the distribution seen in the geostatistical realizations because they are solely based on core data. Therefore, the lack of data for the transitional relationships among all the lithologies is a epistemic uncertainty in the development of the realizations.

However, due to the statistically randomized nature of the realizations, it is also important to note that the realizations do not portray exact conditions of salars. The statistical randomization process utilizes the same spatial proportions of hydraulic conductivity as the hydrostratigraphic framework, but it does not ensure that the produced realizations portray distributions of conductivity that would realistically occur in a salar environment. While the realizations portray realistic likelihoods of transitional relationships among lithologies, the spatial distribution of those relationships are not guaranteed to be accurate when they are randomized. This concept specifically holds true for the model's asymmetrical nature, with evaporite sequences dominating the salar-ward side of the model and alluvial fan deposits comprising the majority of the recharge area. Rather than modeling realistic conditions, this stochastic analysis instead aims to address the role of stratigraphic continuity on the time-sensitive dynamics of brine-to-freshwater interfaces in response to changes in the aquifer's hydrology and specifically to variations in inflow.

1.7 Conclusion

Brine-to-freshwater interfaces control the location of groundwater-fed ecosystems and thus the hydrologic conditions of brine-bearing aquifer due to density-driven circulation and its resulting upwelling of fresh to brackish water to recharge shallow pools and wetlands. However,

homogenous and isotropic numerical models fail to capture the geometry and the dynamics of such interfaces. We therefore assess the extent to which lateral hydrostratigraphic continuity impacts the geometry as well as the time-dependent response of brine-to-freshwater interfaces. To constrain the impact of geologic complexity, we employed a series of geostatistical realizations in SEAWAT numerical simulations to assess their impact on the total distance that the interface travels, the stability of the interface in terms of time required to cease migration, and geometry via the interface slope and observed versus simulated conditions.

The hydrostratigraphic framework of SdA produced a modeled interface that matched observaions within R^2=0.80 while the homogenous model's results diverged from observed values. Responses from the hydrostratigraphic framework were also remarkably stronger in both sensitivity and stability than the homogenous results. Geostatistical realizations support findings from comparison of the SdA's hydrostratigraphic framework and its homogenous counterpart. Simulated values of concentration and hydraulic head best match observed conditions from SdA for the realizations with the strongest trend in horizontal continuity. Results further show a decrease in the slope of the interface as continuity in the realizations increases, indicating that the improved matching of observed and simulated values is linked to the shallowing induced by the increase in continuity. Our findings further show a strong first-order relationship between hydrostratigraphic continuity and brine-to-freshwater interface response dynamics, with interface migration increasing by an order of magnitude and instability increasing by a factor of three when horizontal hydrostratigraphic continuity increases by a factor of two.

These results suggest that geologic complexity and hydrostratigraphic continuity are impact saline intrusion and therefore must be accounted for when modeling at all scales. The degree to which both anthropogenic extraction and ET coupled with hydrostratigraphic

continuity impact interface dynamics remains undefined. However, future modeling initiatives using a similar geostatistical approach can address possible relationships on these different strains to brine-bearing aquifers. Arid regions throughout the world are experiencing strains on groundwater resources as anthropogenic exploitation and climate-driven aridity increases. This modeling approach constrains the sensitivity and stability of brine-to-freshwater interfaces in arid regions in response to climate-driven changes in the hydrologic budget by establishing a first-order control between hydrostratigraphic continuity and density-driven dynamics.

1.8 Summary

Numerical simulations of density-driven groundwater flow along brine-to-freshwater interfaces that utilize equally probable representations of hydrostratigraphic heterogeneity indicate that geometry as well as the sensitivity and stability of interfaces depend on continuity of geologic units. While increased horizontal continuity leads to shallower and more anomalous expressions of the interface, increased continuity also results in higher sensitivity and more instability. Variable flow fields resulting from high hydraulic conductivity flow paths create an unstable environment in which the lack of connectivity prevents the most efficient reaction in an aquifer in response to hydrologic changes. This increases the time required to reach a dynamic steady state by approximately a factor of three as continuity increases in the horizontal direction. The results indicate that developing a hydrostratigraphic conceptualization without identifying both the distribution of conductivity and the location of preferential flow risks the loss of accuracy in interpretations of density-driven fluid dynamics. These findings have implications for accurately assessing the risk of saline intrusion and the sustainability of groundwater-fed shallow pool ecosystems in brine-bearing aquifers.

APPENDIX

USING SALAR DE ATACAMA AS AN ANALOG FOR OTHER ARID BASINS TO ADDRESS GEOLOGIC IMPACTS ON THE DYNAMIC RESPONSE OF BRINE-TO-FRESHWATER INTERFACES

Appendix S1: Introduction to supplementary information

The geologic controls that influence solute transport in density-driven flow in an aquifer remain poorly defined, and therefore brine-to-freshwater interfaces that develop in arid climates have few constraints in terms of how differences in hydrostratigraphy impact their dynamics and stability. Despite the widespread impact of this phenomenon throughout arid regions, the impact of geologic factors on brine-to-freshwater interfaces remains poorly constrained. Geologic conditions such as complex hydrostratigraphy and fault behavior are common features in arid climates thus merit a parametric analysis with 2-D SEAWAT models, which is further explained in section 1.4.4 above. The southeastern transition zone in SdA serves as the hydrostratigraphic basis for the series of geostatistical realizations, with geologic characterization information from over 28 cores and water lever and permeability data from over 15 wells within the transition zone's upper 300 meters. Geostatistic variations based on the available core data from SdA provides insight into the hydrostratigraphic features that impact interface migration and stability, such as the number of high-permeability conduits and the average ratio of change in hydraulic conductivity between hydrostratigraphic units. The below information provides further insight into the interpretation of SdA's hydrostratigraphic framework that served as the basis for the geostatistical realizations.

Appendix S2: Hydrogeologic setting of Salar de Atacama

As a prime example of a salar with a mature halite nucleus, SdA represents the ideal site for investigating interface response to both the hydrostratigraphic and hydrologic mechanisms that determine an interface's architecture. SdA is located in northern Chile, along the southern fringe of the hyper arid Atacama Desert. At over 2,300 meters above sea level (masl), SdA is located in an endorheic basin that has developed a mature halite nucleus of over 1,800 km^3 in volume since the late Miocene (Jordan et al., 2002, 2007). The Monturaqui-Negrillar-Tilopozo (MNT) aquifer provides inflowing freshwater from higher elevation areas relative to SdA (Rissmann et al., 2015). As a mature salar, SdA's halite nucleus is an evaporite series that ranges from 400 to 1,800 m in thickness while the margin is a relatively recent depositional environment where alluvium accumulates with evaporates (Jordan et al., 2007). The aquifer below SdA hosts relatively dense brine (i.e. ~1,200 kg/L) that is distinct in both density and chemistry from fluids entering the system (Boutt, Hynek, Munk, & Corenthal, 2016a; Munk et al., 2016).

SdA's hyper arid climate results from low precipitation that has continued since the Miocene, which likely comprises the world's longest history of aridity in geologically modern time (Clarke, 2006). While SdA is located adjacent to the Atacama Desert, which receives <5 $mm \bullet yr^{-1}$, SdA itself receives between 16-20 $mm \bullet yr^{-1}$ (Jayne, Pollyea, Dodd, Olson, & Swanson, 2016; Bitar Chacra et al., 2010). The high evaporation rates of approximately 0.1 to 2.8 mm/day create a deficiency of input to the hydrologic budget that cannot close without recharge from beyond SdA's topographic divides (Corenthal et al., 2016). The Altiplano-Puna region is located immediately to the east of SdA and provides the main source of recharge via subsurface flow to the basin (Corenthal et al., 2016). Geographically, the Andean Cordillera lies to the north, east,

and south of SdA and defines the majority of the salar's topographical closure. Cordillera de Domeyko rises to above 5,500 masl and represents the remainder of the salar's closure (Reutter et al., 2006). The salar's basin floor, which comprises the surface of the halite nucleus, resides at an elevation of approximately 2,300 m above mean sea level (Munk et al., 2016).

While previous studies created a general stratigraphic characterization for SdA, those studies do not document stratigraphy for the southeastern area of the salar and its margin (Bascuñán et al., 2016; Jordan et al., 2002, 2007). As seen in figure 2, extensive data on the southwestern transition zone of SdA has been collected. Recently gathered geophysical data (i.e. NMR, TEM, and nano-TEM methods), core data, and field observations located throughout the research site provide greater detail on the southeastern area of SdA and the aquifer's transition zone. Field observations from wells in and adjacent to the transition zone are available in table 1. Section 1.5.4 details how data and field observations improve the understanding of SdA's southeastern stratigraphy.

SdA's proximity to the Altiplano-Puna Volcanic Complex has impacted the salar's stratigraphic units and thus its hydrogeologic dynamics. Large-scale volcanism has occurred throughout the region since the Miocene. Present-day hydrothermal activity currently escalates the temperature regime when compared to non-volcanic areas, with temperature profiles ranging between 160-230° C at depth that can increase to 263° C at 800 to 1,000 m below surface grade (Cortecci et al., 2005). Historically, a series of low-permeability ignimbrites developed in the area through Miocene to Pleistocene volcanism (Jordan et al., 2007). Volcanic lithologies in SdA include tuffs and ignimbrites (Jordan et al., 2007; Schmitt, 2001). Several studies note that Miocene to recent volcanism in the region (de Silva, 1989) created the formations of ignimbrite that underly SdA's halite nucleus and partially comprises the basin's slopes (Houston et al.,

2011; Lindsay et al., 2001). Specifically, the Pliocene-age Tucucaro ignimbrite may have low permeability properties due to its ostensibly non-friable and unfractured structure (Rissmann et al., 2015). A study in the Tujayto basin, which is approximately 60 km southeast of SdA, encountered an ignimbrite with low permeability that appeared to define flow dynamics as an aquitard (Herrera et al., 2016). A separate study on a basin in Australia indicates that seepage in brine-rich aquifers controls the rate of salinity increase (Skrzypek et al., 2016); SdA's low-permeability Tucucaro ignimbrite may therefore maintain high salinity concentrations by preventing seepage in its unconfined aquifer, as evidenced by the salar's high salinity rates and distinct interface. The shallow slope of SdA's brine-to-freshwater interface may result from the confining effect of the area's interbedded ignimbrite layers because the extreme difference in anisotropy between stratigraphic units causes the development of preferential pathways in the horizontal direction; however, the extent to which the ignimbrite impacts the geometry and migration of the interface remains unexplored.

Along with volcanics, regional tectonics impact the area's hydrogeology. Located within the northern Andes' forearc, SdA represents a tectonic basin that originated from late Cretaceous inversion of the Jurassic to early Cretaceous extensional Tarapacá backarc Basin (Jordan et al., 2007). The area's inversion resulted from late-Cretaceous and Paleocene shortening, but then during the Oligocene to early Miocene the area experience another period of extension (Mpodozis et al., 2005). As a result, SdA subsided and created a series of normal faults along the eastern edge of the salar; the fault system coincides with the present-day location of many of SdA's surface water bodies (Jordan et al., 2007; Reutter et al., 2006). Despite the documented faulting from the above-described basin extension, it is unclear how faulting impacts the interface's geometry and dynamics.

While SdA's margin and surrounding stratigraphy includes ignimbrites consistent with the region's volcanism, SdA's stratigraphy primarily comprises evaporite facies and clastic alluvial deposits that represent the weathering of the above-described upgradient volcanic lithologies (Bobst et al., 2001; Lowenstein et al., 2003). With the Atacama Desert experiencing arid conditions since the late Jurassic period (150 Ma), sedimentary deposition in SdA primarily consists of alluvial fan deposits (A. Hartley et al., 2005). Generally, evaporites and carbonates from the Pliocene and late Miocene overlie conglomerates and ignimbrites from the Oligocene to lower Miocene Paciencia group (Jordan et al., 2007). While several studies document the area's stratigraphy, the area's tectonic regime coupled with alteration from the brine's geochemical reactions complicates the procession of the formations and produces variation throughout the salar's extent. A comprehensive review of the area's hydrogeology therefore requires extensive subsurface stratigraphic characterization to accurately assess those variations.

As shown in Figure 2, surface water bodies in arid basins occur in areas that are conducive for groundwater upwelling and require a combination of merging conditions including relatively high hydraulic conductivity and high evaporation (Tyler et al., 2006). SdA's surface water bodies provide the main source of evaporation in the basin as surface water bodies (Tejeda et al., 2003). Located along the halite margin, as seen in figure 13, the lagoons exist within the margin of the halite nucleus in the southeastern section of SdA. Among the surface water bodies in the southeastern margin of SdA, there are two distinct geographic systems: the Salada-Saladita-Interna (SSI) lagoon system and the Punta-Brava lagoon system. Spring-fed streams provide a portion of the recharge to the SSI lagoon system while no evident streams feed into the Punta-Brava lagoon systems. While the above mentioned surface water bodies experience seasonal variation in inundation, there are also groups of open pools along the border between

SdA's halite nucleus and the margin in the southeastern area that disappear on a sporadic annual basis. While variations in recharge impact inundation levels, the factors that impact seasonal variations remain unconstrained.

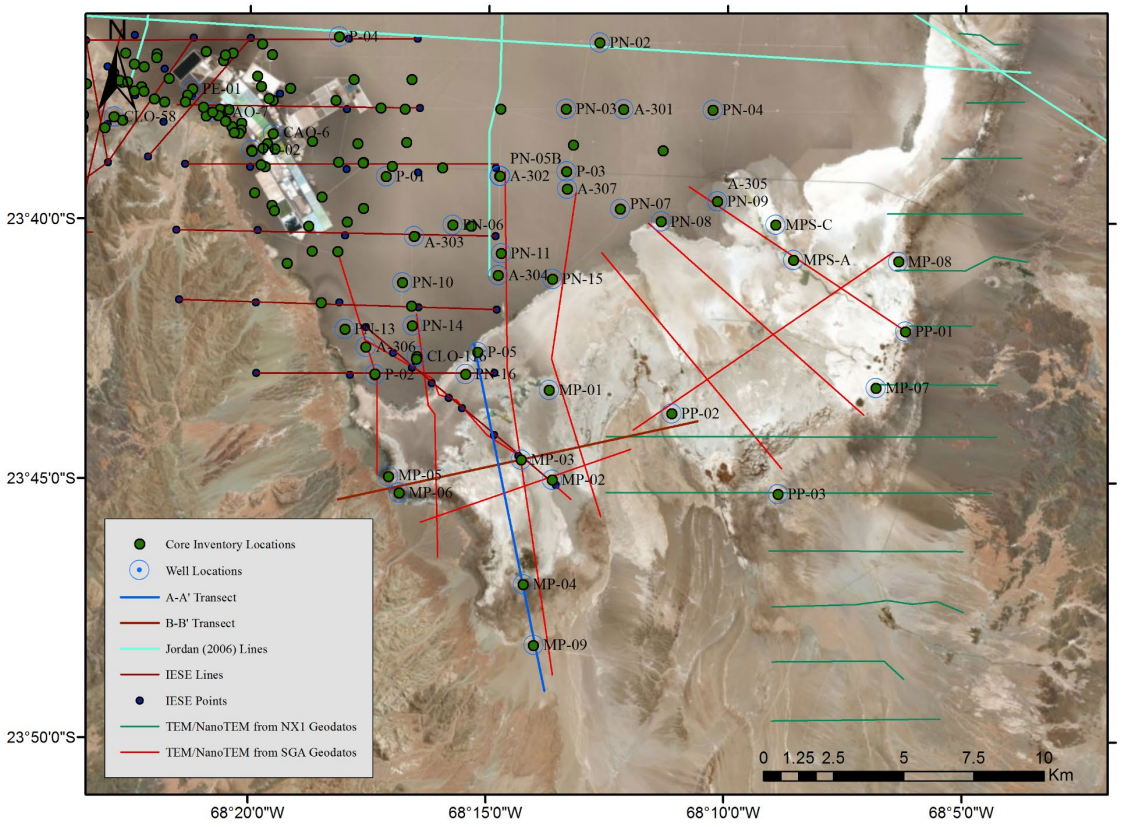

Figure 14 A site map of the southeastern margin of Salar de Atacama in northern Chile. The green points are the core locations and the blue points are the well locations to date. The blue line represents the A-A' cross section and the location of hydrostratigraphic framework for the 2-D numerical models. The wells are labeled. The red line represents the B-B' cross section. The orange and green lines represent the locations of geophysics surveys.

WID	Easting	Northing	Elevation	Bottom of Screen	Hydraulic Head	Specific Conductivity	Density
	WGS84		masl	masl	masl	(µS/cm)	Kg•L^{-1}
MP-01A	578647.25	7376428.92	2300.73	2293.78	2300.72	35620	1.02
MP-01B	578649.72	7376429.64	2300.69	2270.44	2300.72	248890	1.21
MP-02A	578746.60	7373235.48	2302.78	2290.86	2302.36	12442	1.00
MP-02B	578744.25	7373235.95	2302.74	2250.82	2299.34	241550	1.20
MP-03A	577649.97	7373947.40	2302.07	2289.67	2302.01	8316	0.99
MP-03B	577653.39	7373946.78	2302.08	2271.68	2302.00	243302	1.20
MP-04A	577716.24	7369509.31	2308.10	2266.79	2307.66	4229	0.99
MP-04B	577716.82	7369513.15	2308.03	2226.44	2299.47	241213	1.20
MP-05A	572915.06	7373355.70	2302.74	2282.63	2301.79	28117	1.01
MP-05B	572912.64	7373356.01	2302.70	2242.79	2301.39	247902	1.21
MP-06A	573298.46	7372778.28	2304.81	2274.91	2303.91	11723	1.00
MP-06B	577653.39	7373946.78	2304.77	2240.14	2299.43	234671	1.20
MP-07A	590305.42	7376506.83	2306.09	2286.08	2305.57	NA	NA
MP-08A	591099.11	7380992.66	2303.48	2281.66	2302.49	NA	NA
MP-09A	578077.00	7367346.00	2318.05	2288.03	2309.19	NA	NA
MP-12A	596116.00	7390800.00	2315.78	2268.29	2306.91	NA	NA
P-05	576091.11	7377780.40	2299.36	2199.49	2298.80	239562	NA
PP-01	591348.31	7378506.54	2305.15	2204.731	2305.091	288000	1.25
PP-02	583007.26	7375593.66	2303.62	2218.77	2300.38	192100	1.16
PP-03	586802.95	7372719.02	2308.68	2189.743	2308.693	189600	1.16
PN-16	575656.17	7377001.21	2299.78	2295.636	2299.706	198490	1.16
BZTP1	578502.94	7367614.72	2319.27	2221.265	NA	4042	0.99
BZTP2	578497.24	7368805.38	2310.87	2230.865	NA	9101	0.99
BZTP3	578925.00	7366867.98	2325.66	2207.66	NA	2855	0.99
TM1	580196.00	7372881.00	NA	NA	NA	1001	0.99
TM2	578116.32	7367621.59	2318.10	NA	NA	3702	0.99
TM6	580451.01	7362009.42	2417.02	NA	NA	2577	0.99

Table 6 Compiled list of available wells located in or adjacent to the southeastern transition zone of Salar de Atacama that provide information on the hydraulic head and/or salinity of the groundwater.

Appendix S3: Modern and Paleo-Hydrologic Setting of Salar de Atacama

SdA exists in a hyper-arid climate that results from its location in the subtropical high pressure zone combined with the orographic barrier of the Andean Cordillera. The barrier, coupled with the east Humboldt current, usually diverts precipitation away from the Atacama Desert and, by proximity, from SdA (A. Hartley et al., 2005; A. J. Hartley & Chong, 2002). The majority of precipitation occurs during the austral summer and larger events that correlate with La Niña years (Houston, 2006b). SdA experiences an average precipitation of 16-20 mm•yr^{-1} while higher elevation in the Altiplano-Puna region directly to the east receive an average of 300 mm•yr^{-1} (Dorsaz et al., 2013; Houston, 2006b). Precipitation in the Altiplano-Puna includes

approximately 50 mm to 80 mm of snow-water equivalent (SWE) in areas above 4,500 masl (Vuille & Ammann, 1997). Based on insolation in the area, a majority of the total annual precipitation likely sublimates and therefore provides little recharge to its aquifer (Vuille & Ammann, 1997).

Since recharge usually occurs for areas that receive 120 $mm \bullet yr^{-1}$ or more, the Altiplano-Puna region at over approximately 3,500 masl represents the closest upgradient area that currently provides a continuous recharge source to the SdA system (Houston, 2006b, 2009). The majority of groundwater recharge for the aquifer therefore exhibits interbasin flow to enter SdA from the Altiplano-Puna region [*Boutt et al.*, 2016; *Corenthal et al.*, 2016]. High-amplitude precipitation events that occur on a semi-decadal frequency also likely perform a key role in recharge to SdA's system (Houston, 2006b; Placzek et al., 2009). Changes in SdA's lagoon inundation reflects these recharge events both seasonally and on the semi-decadal scale (figure 15).

While paleoclimate records indicate that SdA has remained arid since the mid-Jurassic at approximately 150 Ma, the region also experienced variability in the Pleistocene glacial eras (Bobst et al., 2001). Glacial lake records indicate that precipitation rates were elevated during glacial periods (Blard et al., 2011; Blodgett et al., 1997; Fritz et al., 2004; Saez et al., 2016). Based on paleoclimate records, the Holocene also exhibited higher precipitation values (Betancourt, 2000; Bobst et al., 2001; Lowenstein et al., 2003). The paleohydrologic variation in precipitation and therefore in recharge likely created elevated hydrologic head that has since decayed to present levels and continues to decay based on the extended aridity of the region (Gayo et al., 2012; Godfrey et al., 2003).

Surface water bodies in SdA exhibit either perennial or seasonal characteristics depending on several factors that include their connectivity with groundwater recharge. As seen in figure 15, which shows the surface water response to a large precipitation event, these divergent temporal characteristics appear with seasonal fluxes in recharge and inflow. The precipitation and flooding event that occurred in SdA on March 24 and 25, 2015 doubled the southeastern region's inundation in seasonal ponding, which mainly resulted in the growth of seasonal surface water bodies. Figure 3 shows how the annual surface water bodies are located in the margin while the fluctuating bodies primarily pool along the margin-nucleus border. The phenomenon of perennial surface water bodies persisting in specific locations supports the developing consensus that persistent surface water in arid basins adjacent to the Andes region depends on groundwater inflow (Houston, 2009). Seasonal bodies that occur in separate locations suggest that these systems have distinct hydrologic responses from the perennial bodies.

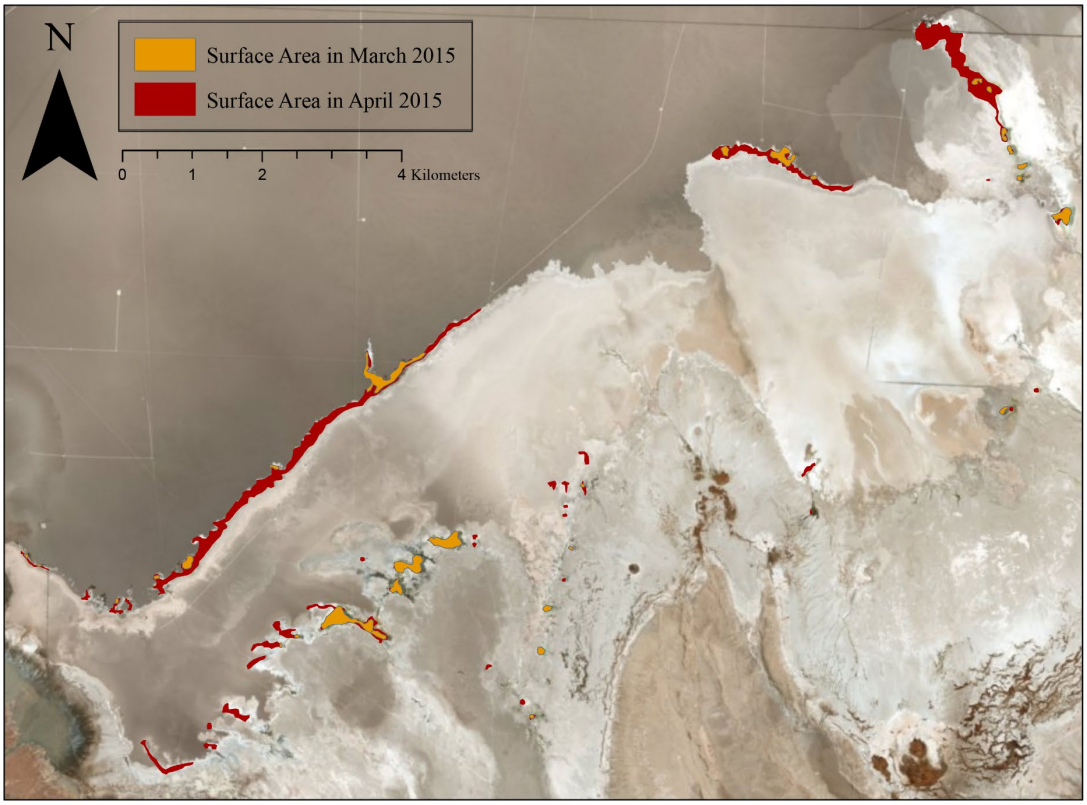

Figure 15 Map of the southeastern margin of Salar de Atacama showing the difference in inundation of the surface water bodies before and after a major precipitation event.

Appendix S4: Information and data from available cores in the transition zone

A series of 27 cores have been extracted from throughout the southeastern margin of SdA between 2013 and 2018, as seen in figure 14 and listed in table 7. These cores were visually examined and assessed for lithostratigraphic identification at the meter scale in three different field excursions in November 2014, October 2017, and December 2017. The meter-scale stratigraphic columns were produced from this assessment, as shown in figures 16 through 18. Note that the shown figures do not encompass all stratigraphic columns considered for the development of the geologic interpretation; the figures include the core locations that are located along the cross section A-A' that was chosen as the basis for the SEAWAT model. These

columns were then converted into simplified core logs that were separated into lithologic categories in order to develop further interpretation for geologic conceptualization. Five primary units have been identified in the observations of available core in the area: pyroclastics (i.e. ash and ignimbrite), alluvial clastics, carbonates, gypsum, and halite. These units are consistent with the known geologic history of the area as described in section S2.

Assessment included observations of color, hardness, grain size, taste, and effervescence under hydrochloric acid. Other observations of the units that were considered included properties for high permeability (e.g. vugs in the carbonate units), indications of brine alteration, and any other unique identifiers and characteristics that may improve the correlation of units among the available cores (i.e. inclusions and parent matrix material). Challenges in lithostratigraphic identification include the extreme alteration from brine, the transitionary nature of the evaporite sequences, and the extremely variable nature of evaporites due to yearly, decadal, and centennial variations in climate, as well as the complex structural environment of the salar previously described in section 1.3.4.

BID	Easting	Northing	Elevation	Core Length
	WGS84		Masl	m
PP-01	591348.31	7378506.54	2305.15	101
PP-02	583007.26	7375593.66	2303.62	85
PP-03	586802.95	7372719.02	2308.68	120
MPS-A	587361.34	7381052.48	2299.75	34
MPS-C	586726.44	7382313.36	2299.13	43
P-02	572432.91	7376977.18	2300.00	28
P-05	576091.11	7377780.40	2299.36	100.5
PE-01	565938.11	7387144.06	2300.11	100
PE-02	568031.96	7384972.22	2300.41	101
PN-02	580457.52	7388790.01	2299.62	11.25
PN-04	584482.74	7386394.70	2299.64	11
PN-05	576891.21	7384047.67	2300.25	50
PN-08	582637.68	7382423.58	2300.13	50
PN-09	584649.77	7383143.48	2299.17	12
PN-13	571361.23	7378596.81	2299.89	12
PN-14	573767.49	7378720.47	2299.87	51
PN-15	578762.48	7380378.39	2299.93	12
PN-16	575656.17	7377001.21	2299.78	50
MP-01	578649.72	7376429.64	2300.69	30
MP-02	578744.25	7373235.95	2302.74	50
MP-03	577653.39	7373946.78	2302.08	30
MP-04	577716.82	7369513.15	2308.03	120
MP-05	572912.64	7373356.01	2302.70	80
MP-06	577653.39	7373946.78	2304.77	81.4
MP-07	590305.42	7376506.83	2306.09	101
MP-08	591099.11	7380992.66	2303.48	63
MP-09	578077.00	7367346.00	2318.05	100

Table 7 Compiled list of core inventory that was reviewed and described, with borehole identification number (BID), location coordinates, elevation, and total length of recovery. A total of 1,760.75 m of core were reviewed for the purposes of creating a hydrostratigraphic framework for the southeastern transition zone of Salar de Atacama.

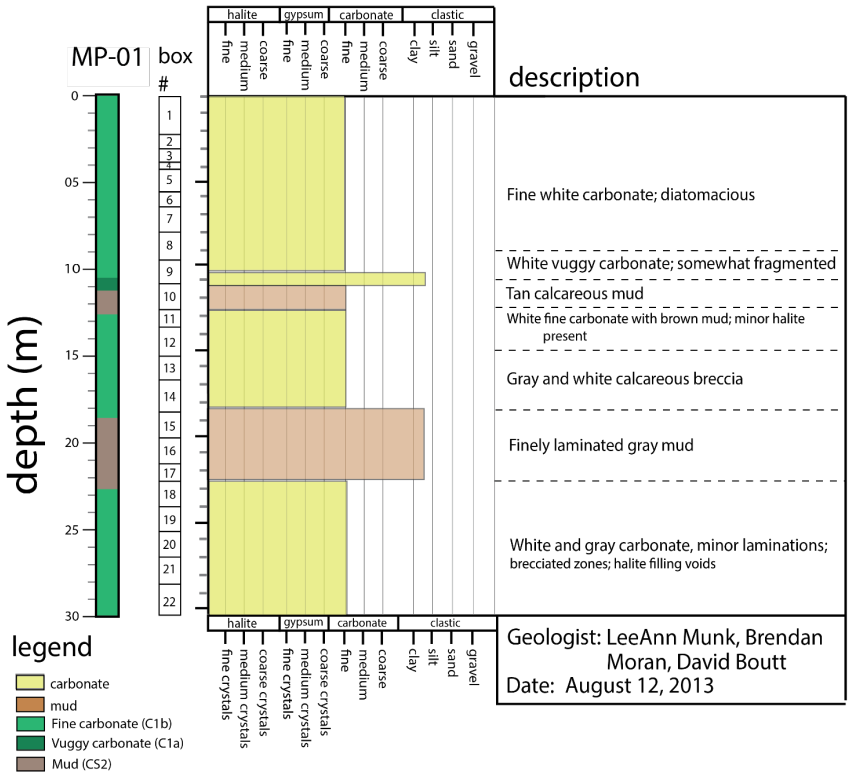

Figure 16 Simplified lithologic log with the stratigraphic column for core MP-01. The stratigraphic columns were developed from visual assessment of the available core and subsequently converted to a simplified log seen on the left for further geologic interpretation.

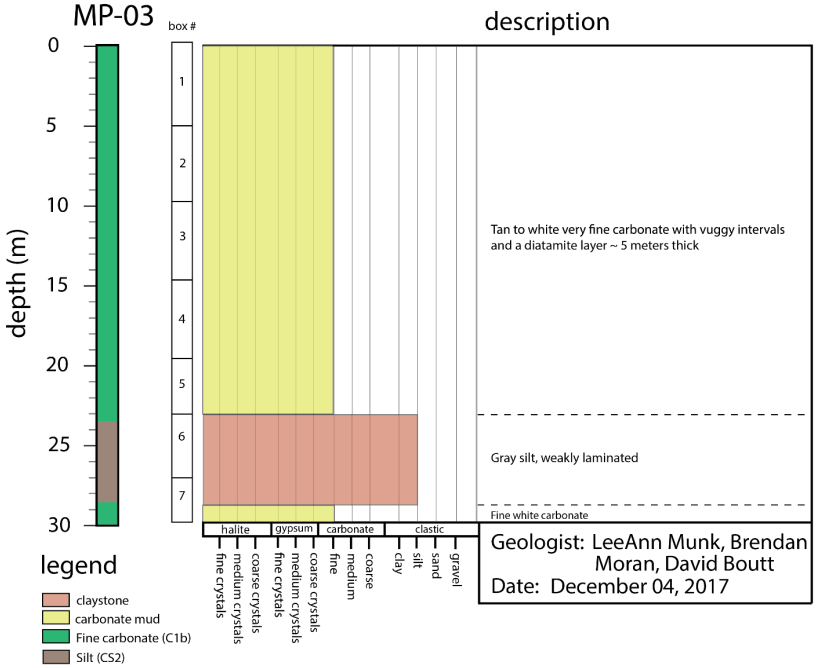

Figure 17 Comparison of simplified core log with the stratigraphic column for core MP-03. Note that MP-02 and MP-03 are very similar and the MP-02 stratigraphic column is therefore not necessary.

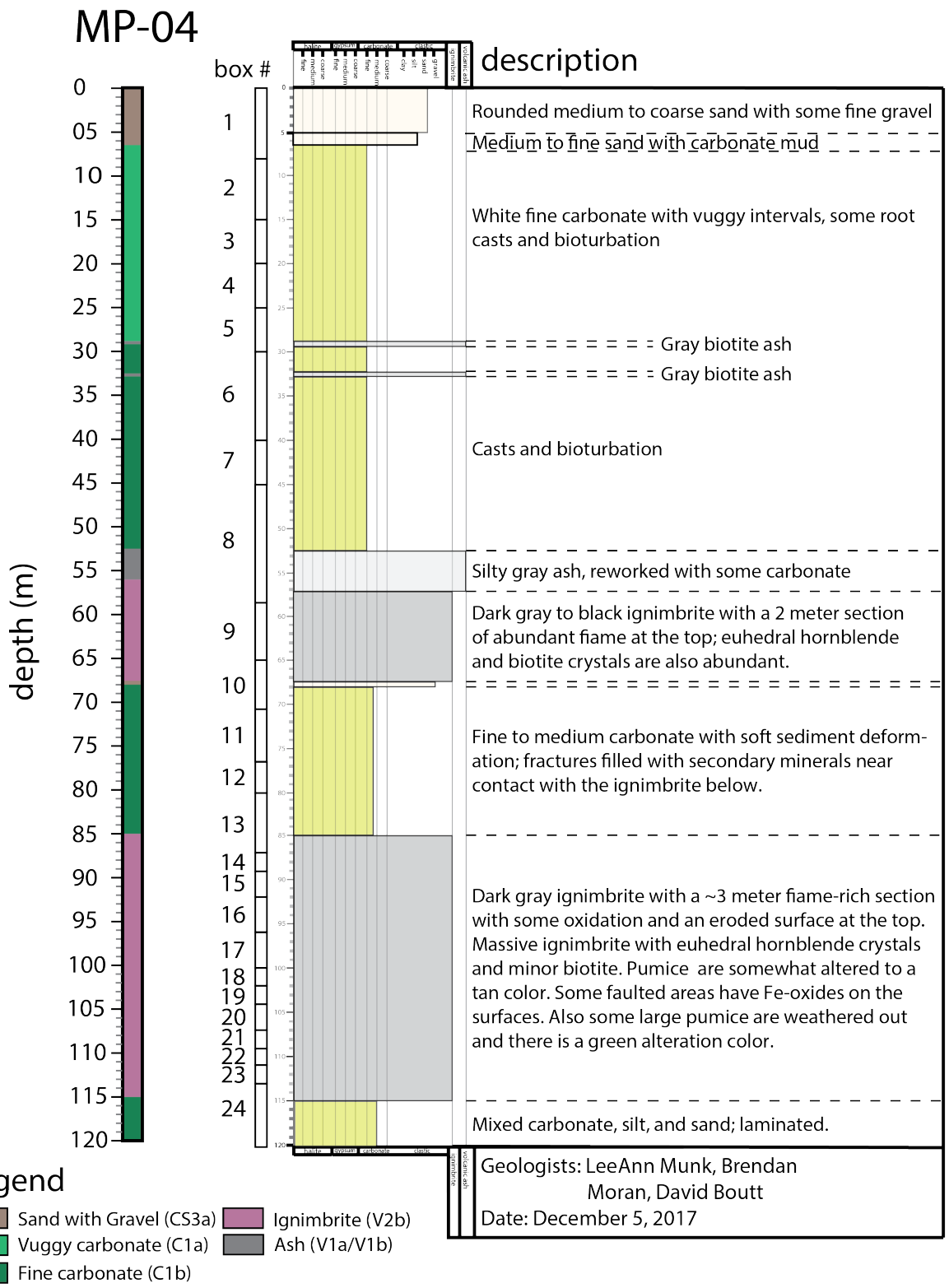

Figure 18 Comparison of simplified core log with the stratigraphic column for core MP-04. Note that this is the deepest core for the study site. Also note that ignimbrite appears twice in this core, exhibiting evidence of folding.

Appendix S5: Geologic interpretation of the southeastern transition zone area of Salar de Atacama

Based on the available lithostratigraphic observations from 27 above-described cores, TEM/nano-TEM assessments, surficial geology information, structural geology information, and background knowledge from literature on the region's geology, a series of interpretations on the transition zone's geology were developed in the form of two-dimensional conceptual cross sections. As seen in figures 19 and 20, cross section A-A' chosen for this 2-D model conceptually depicts the most current and comprehensive geologic interpretation of the distribution of lithologies. Cross section A-A' also runs parallel to projected flow in the aquifer based on calculations from field measurements of piezometric head for the available inventory of wells. The geologic conceptualization is based on a synthesis from the above-described data as well as reasonable interpretations based on background knowledge of the region's geology in areas that lack core data. The units in the 2-D conceptual model represent lithologies with similar observations of composition, permeability, and friability. As seen in the map in figure 13, the cross section is located in the southeastern transition zone of SdA and is oriented parallel to projected groundwater flow into the basin, as extrapolated from groundwater head gradients.

The conceptual model is constrained by meter-scale lithostratigraphic interpretation from the cores, as seen in figures 16 through 18 and as previously described in section 1.5.1. Meter-scale assessment admittedly does not capture how the composition of evaporite sequences exhibit high variation in composition and in spatial distribution on the sub-meter scale. While meter-scale assessment likely does not capture the extremely variable and transitional nature of the evaporite sequences in the southeastern margin of the salar, the observed hydraulic properties likely remain consistent on the meter scale (Gelhar et al., 1992). This is especially true for the

purpose of this study's proposed modeling, which has a finite grid scale of 10 meters in depth and requires further simplification and merging of lithological interpretations.

The geologic conceptualization also integrates an exhaustive review of SdA's known faults and depicts the salar's compressional environment and recent tectonic history of reverse faulting. Geophysical assessments have confirmed the likely existence of an east-west trending normal fault that exists in the southern area of the cross section between MP-04 and MP-09. The second fault projected in the cross section is also normal and likely trends in the east-west direction. While this fault has not been substantiated by geophysical assessments, its presence is highly likely based on the spatial variation in lithological sequences between MP-04 and the other core data as well as the known prevalence of faulting in the area (Reutter et al., 2006).

Several uncertainties regarding the area's geology results in data gaps for the conceptual model. Generally, since our deepest core MP-04 ends at 120 meters, a lack of information for the transition zone area 120 m below surface grade permits only a crude assessment of the lithological distributions at depth. Based on knowledge of regional geology, the most reasonable conjecture is that the Vilama Formation is present below the Tucucaro ignimbrite. Despite the data gaps, this represents the most advanced and comprehensive assessment of the area's stratigraphy and structural conceptualization to date. Lack of data on the full extent of faulting in the area also limits the model's structural accuracy; however, new geophysical seismic surveys being conducted this year in the southern area of the salar may have implications for the extention of faults from the salar into the transition zone.

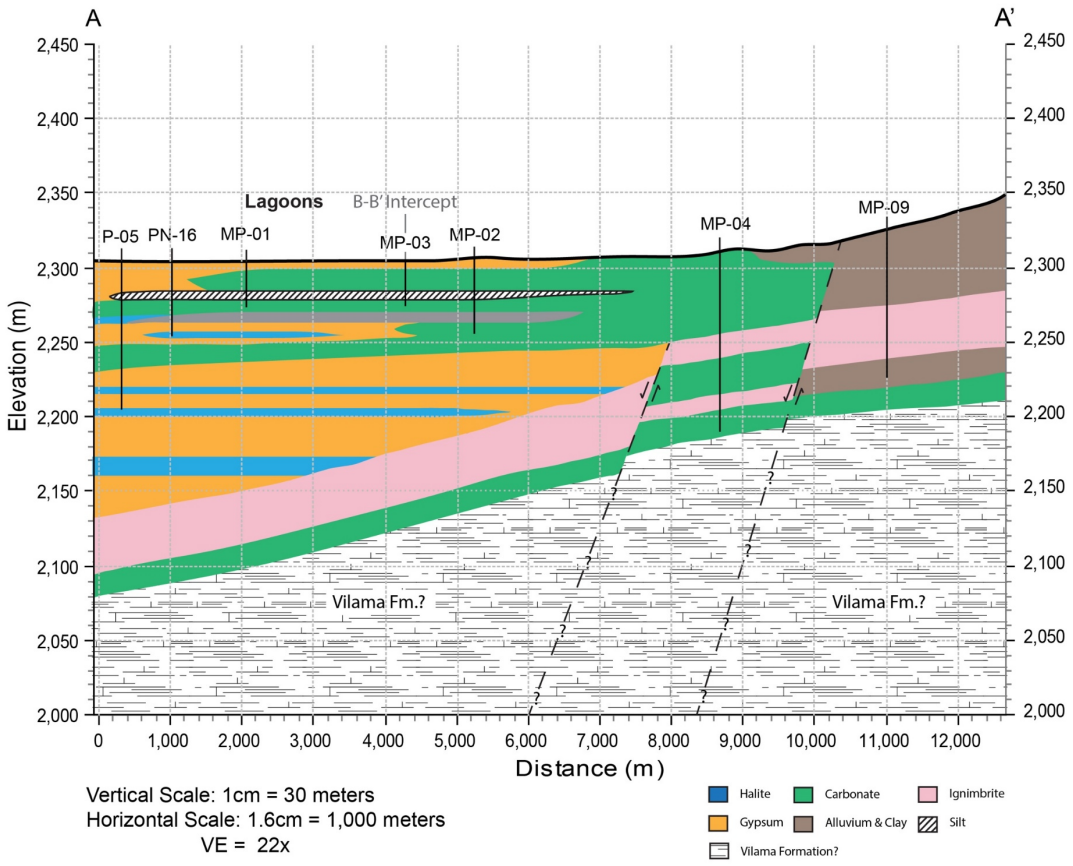

Figure 19 Geologic conceptual model of cross section A-A' as shown in figure 4, with lithologies distinguished as halite, carbonate, ignimbrite, gypsum, a specific silt layer that likely forms a strong aquitard, and clastic material primarily composed of alluvium and clay. Below the extent of exploration is the likely continuation of the Vilama Formation.

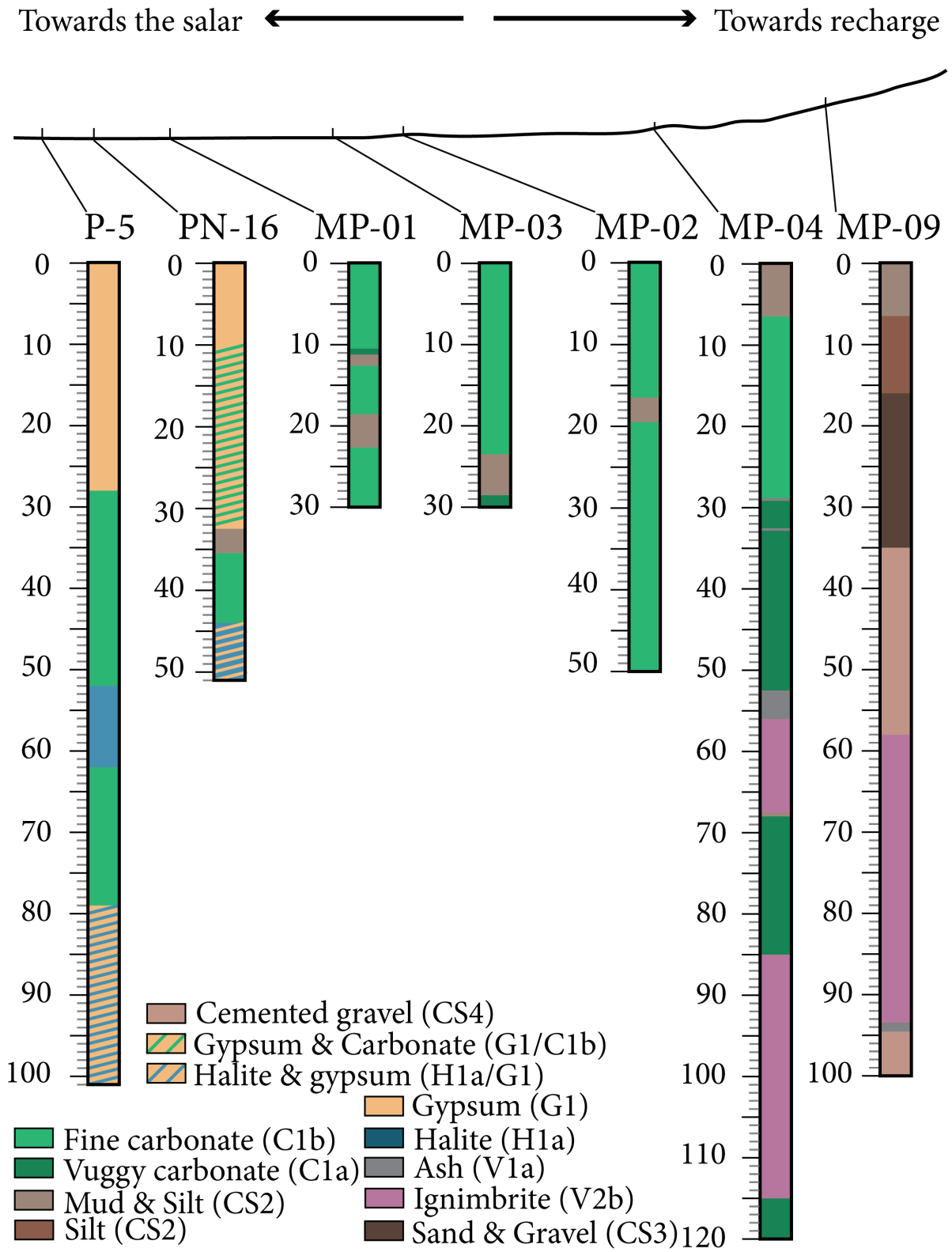

Figure 20 A comparison of simplified core logs for the multipiezometers (MPs) located along the modeled cross section of SdA. The topographic profile is extracted from the 10-m resolution digital elevation map available for SdA. Colors are correlated to lithostratigraphic units. Note that the MPs serve as observation points for the models.

Appendix S6: Hydrogeologic data

A collection of hydrogeologic data from both previous work and recent field excursions for this project have developed an extensive documentation of the transition zone's hydrogeologic conditions (table 8). Results from the over 50 tests performed are available. The listed series of multi-piezometer (MP) wells, with locations shown in figure 13, have been routinely assessed for hydraulic head over a period of ten years. All MP wells have also been tested for permeability using LeFranc and slug tests; other shallow wells in the southeastern TZ have also produced conductivity values through pump tests. TEM/nanoTEM profiles and continuous specific conductivity measurements (figure 22) for the MP wells constrain the depth of the brine-to-freshwater interface in the transition zone. For the purpose of this thesis, currently utilized data is limited to hydraulic head, salinity, density, and permeability values; however, other data sets such as temperature and water chemistry are available for the above mentioned points which are beyond the scope of this thesis but provide critical insight into the complexity of the region's hydrologic budget and groundwater flow dynamics.

WID	Test Depth Top	Test Depth Bottom	HK (m/d)	Lithology
P-01	9	10	0.08	Halite (H1a)
P-02	24	25	0.04	Halite (H1a)
P-03	23	24.2	0.60	Halite (H1a)
P-04	24.8	25.8	0.43	Halite (H1a)
P-05	29	30	0.06	Halite (H1a)
P-06	40.9	41.9	0.16	Halite (H1a)
P-07	4	5	0.39	Halite (H1a)
P-08	14	15	0.43	Halite (H1a)
P-09	19	20	1794.00	Halite (H1a)
P-10	24	25	0.72	Halite (H1a)
P-11	29	30	3.81	Halite (H1a)
MP-02	9	10	237.00	Fine carbonate (C1b)
MP-03	10.9	12.5	68.90	Fine carbonate, vuggy (C1a)
MP-03	15	16	66.00	Fine carbonate, vuggy (C1a)
MP-03	29	30.5	0.41	Fine carbonate (C1b)
MP-01	6.3	7	136.00	Fine carbonate (C1b)
PN-16A	0	30	233	Gypsum/Carbonate (G1/C1b)
PN-16B	0	30	276.6666667	Gypsum/Carbonate (G1/C1b)
PN-16A	0	30	266.6666667	Gypsum/Carbonate (G1/C1b)
PN-16B	0	30	400	Gypsum/Carbonate (G1/C1b)
PN-16A	0	30	276.6666667	Gypsum/Carbonate (G1/C1b)
PN-16B	0	30	333.3333333	Gypsum/Carbonate (G1/C1b)
MPS-AA	3.20	4.00	0.30	Gypsum (G1)
MPS-AB	29.00	30.70	0.00	Fine carbonate (C1b)
MPS-CA	2.55	3.40	91.80	Gypsum (G1)
MPS-CA	39.10	40.00	60.40	Gypsum/Carbonate (G1/C1b)
MPS-CA	2.55	3.40	3.38	Gypsum (G1)
MPS-CA	39.10	40.00	3.09	Gypsum/Carbonate (G1/C1b)
P-02	27.00	28.00	0.31	Halite (H1a)
PN-14	0.00	50.00	5550.00	Halite (H1a)
TPZ-10	1.00	2.00	2.98	Gypsum (G1)**
TPZ-11A	1.00	2.00	0.10	Gypsum (G1)
TPZ-11B	1.00	2.00	0.66	Gypsum (G1)
TPZ-11C	1.00	2.00	1.25	Gypsum (G1)
TPZ-12	1.00	2.00	2.13	Gypsum (G1)**
TPZ-13C	1.00	2.00	0.31	Gypsum (G1)
TPZ-1A	1.00	2.00	0.63	Gypsum (G1)**
TPZ-1C	1.00	2.00	1.13	Gypsum (G1)**
TPZ-1B	1.00	2.00	0.28	Gypsum (G1)** ***
TPZ-2A	1.00	2.00	7.08	Fine carbonate (C1b)

TPZ-2C	1.00	2.00	0.35	Fine carbonate (C1b)
TPZ-4	1.00	2.00	1.30	Gypsum (G1) **
TPZ-5A	1.00	2.00	1.06	Gypsum (G1) **
TPZ-5B	1.00	2.00	0.21	Gypsum (G1) **
TPZ-6	1.00	2.00	3.29	Gypsum (G1) **
TPZ-7A	1.00	2.00	0.36	Gypsum (G1)**
TPZ-7B	1.00	2.00	3.35	Gypsum (G1)**
TPZ-8	1.00	2.00	0.51	Gypsum (G1)**
TPZ-9A	1.00	2.00	0.01	Gypsum (G1)**
TPZ-9B	1.00	2.00	0.30	Gypsum (G1)**
TPZ-9C	1.00	2.00	1.92	Gypsum (G1)**
TPZ-13A	1.00	2.00	0.34	Gypsum (G1)
TPZ-13B	1.00	2.00	0.32	Gypsum (G1)
Tucucaro	1*	2.00	15.60	Clastic (CS2)
PN-08	2.00	30.00	7280.00	Gypsum (G1)
CL-06	1.00	2.00	453.00	Gypsum (G1)
MPW-01	0.00	300.00	1.40	Clastic (CS2)

Table 8 Available hydraulic conductivity values collected from pumping tests in the research site area and correlated to the dominant lithologies in the southeastern transition zone area.

Appendix S7: Hydrostratigraphic interpretation

In order to assess the impact of geologic heterogeneity to interface dynamics and sensitivity, a hydrostratigraphic framework (HSF) for SdA has been developed. Based on the geologic interpretation described in section 1.5.2, the lithostratigraphic units from that interpretation have been converted into hydrostratigraphic units. The distribution of hydraulic conductivity values for the current HSF for SdA, as depicted in figure 21 and in table 3, are based on the available permeability values discussed in section 1.5.3. These permeability values were correlated to the lithostratigraphic unit in which each test occurred. The values for each lithostratigraphic unit were then analyzed for statistical average as well as the standard deviation. The hydrostratigraphic framework represents a possible value for each lithostratigraphic unit within one standard deviation of the average value for the unit. The five assigned lithostratigraphic units were assigned a range of HK values that vary by five orders of magnitude, which is within the range of realistic hydrogeologic conditions as evidenced by the

range of pump test results in table 8. The HSF along with the geostatistical realizations of the HSF then experienced the set of hydrologic conditions that are further described below in section 1.5.7.

The current conceptualization of the hydrogeologic environment of SdA's southeastern transition zone includes a confined aquifer, with the low-HK ignimbrite unit representing the Tucucaro ignimbrite serving as the primary confining aquitard. As seen in figure 22, calculations on the aquifer's potentiometric pressure head confirm that confined conditions do exist, and further suggests that a series of aquitards may exist at varies depths in the aquifer. While MP-04 may provide insight into possible confining conditions resulting from the ignimbrite, several other MP wells portray similar conditions despite having shallower depths. A distinct silt layer runs throughout the transition zone area at a depth of between 15 to 25 meters below surface grade; this silt layer may have low enough transmissivity properties to serve as another aquitard, which thus suggests that a complex series of confining conditions impact the groundwater flow in the aquifer. These observations thus warrant an investigation into the effect of the continuity on the dynamics of confining conditions and how those dynamics impact interface sensitivity to climatic changes in hydrology.

It is acknowledged that this hydrostratigraphic framework does not incorporate laboratory analyses of porosity and pore throat values for any samples from the research site. This represents a data gap in the understanding of the hydrogeology of the area. However, despite this deficiency in data, it is important to note that the scale of the modeling does not require pore-scale analysis and that for modeling purposes such analyses would serve as a secondary constraint compared to the hydraulic conductivity values gathered from available pump test values (Gelhar et al., 1992). Furthermore, nuclear magnetic resonance (NMR) results provide a

means for assessing smaller scale permeability values and provide constraints and support for the determined values in the hydrostratigraphic framework. Table 3 provides a range of possible hydraulic conductivity values from the NMR data and figure 22 provides a visual representation of the composite results from the NMR analysis. While hydrogeologic interpretations from NMR have some uncertainty due to changes in specific storage and compaction, comparisons between NMR and pore throat analysis indicate that NMR provides a reasonable estimation for hydraulic conductivity values on a larger scale and provides more insight into the spatial distribution of changes in hydraulic conductivity (Xiao et al., 2017).

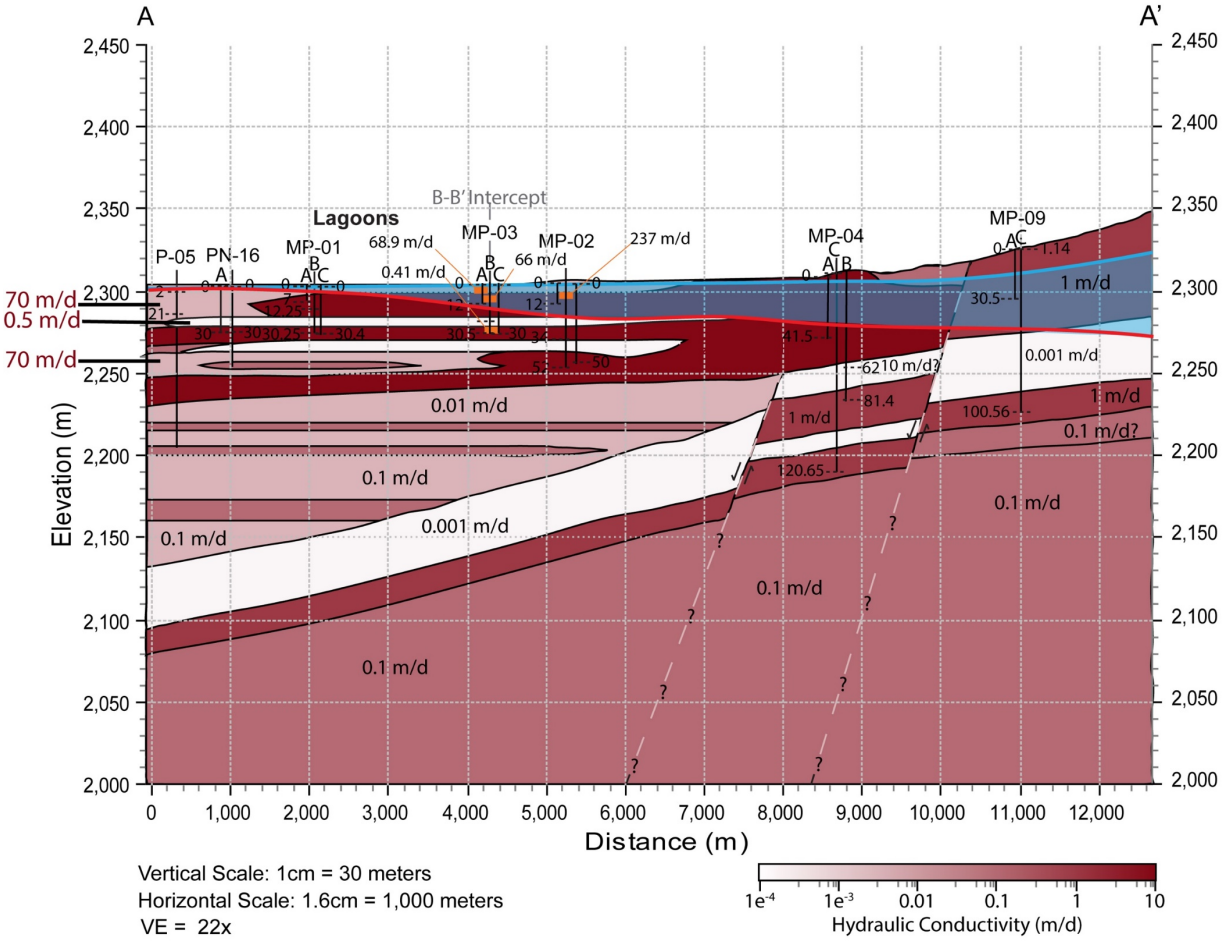

Figure 21 Conceptualization of hydrostratigraphic framework with colorized logarithmic scale. Note that red and blue lines represent the interpreted location of the brine-to-freshwater interface and the water table, respectively.

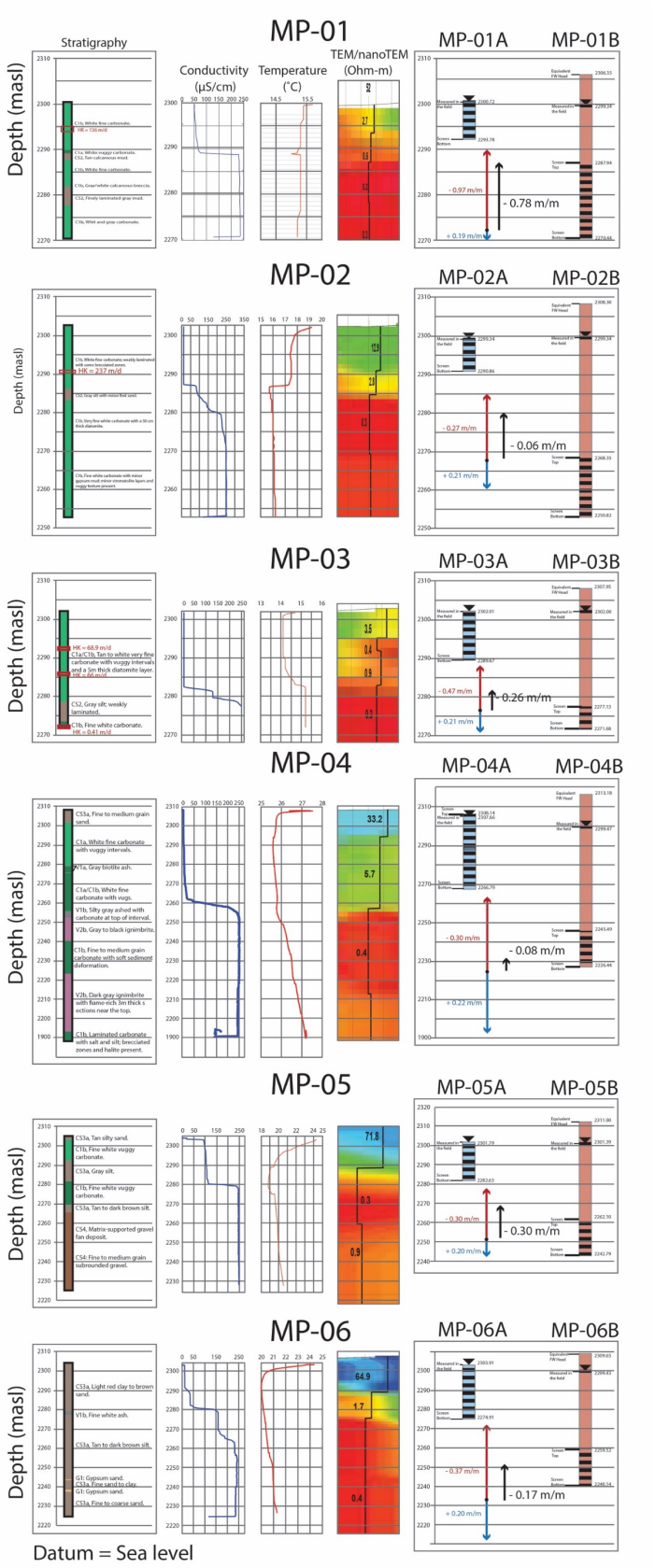

Figure 22 Comparison of core logs, temperature, specific conductivity, and pressure head with depth.

Appendix S8: Hydrologic data

The model's boundary conditions have been constrained based on the available hydrologic data for SdA and on previously developed and accepted knowledge of arid hydrology. The closest weather station is located in Peine; recharge estimates are based on precipitation data from Peine as well as TRMM estimates. Inflow estimates from the MNT aquifer are based on estimates from previous studies (Anderson et al., 2002; Corenthal et al., 2016; McCartney, 2001). Evapotranspiration estimates noted in table 9 are based on previous work from Corenthal et al. (2016) as well as recent industrial reports and other previous studies (Houston, 2006a; Kampf et al., 2005; Kampf & Tyler, 2006; Mardones, 1986). As further explained in section 1.6.6, the collected values were then averaged as seen in table 10, and the final ET value for the model was calculated as a weighted average based on the extent of each lithological surface intersecting the modeled area.

Source	Inflow Maximum and/or Average ($m^3 \cdot d^{-1}$)	Inflow Minimum. ($m^3 \cdot d^{-1}$)
Corenthal et al. (2016)	319.86	N/A
Anderson et al. (2002)	972	432
McCartney (2001)	432	388.8

Table 9 Inflow estimates from available literature, as recalculated to proportionally match the dimensions of the model's cross section.

Source	ET ($m \cdot d^{-1}$)	Area
Golder (2017)	0.0095726	Vegetated wetland
Kampf (2005)	0.0004	Halite-gypsum margin crust
Kampf (2005)	0.0006	Halite-gypsum margin crust
Kampf (2005)	0.0011	Carbonate margin
Kampf (2005)	0.0028	Vegetated wetland
Kampf (2005)	0.0004	Vegetated wetland
Kampf (2005)	0.0011	Vegetated wetland
Mardones (1986)	0.0002	Alluvial Fan
Mardones (1986)	0.00019	Carbonate margin
Mardones (1986)	0.00013	Carbonate margin
Mardones (1986)	0.00045	Vega
Mardones (1986)	0.00057	Alluvial fan
Mardones (1986)	0.00211	Alluvial fan
Kampf and Tyler (2006)	0.001000166	Vegetated wetland
Kampf and Tyler (2006)	0.00611712	Lagoon
Kampf and Tyler (2006)	0.02014848	Alluvial fan
Kampf and Tyler (2006)	0.00062208	Halite nucleus
Kampf and Tyler (2006)	0.00048384	Halite nucleus
Kampf and Tyler (2006)	-0.00010368	Halite nucleus

Kampf and Tyler (2006)	0.00141696	Halite nucleus
Kampf and Tyler (2006)	0.00307584	Carbonate margin
Kampf and Tyler (2006)	0.00114048	Carbonate margin
Houston (2006)	0.006	Lagoon
Houston (2006)	0.000410046	Carbonate margin
Houston (2006)	6.0274E-05	Halite nucleus
Houston (2006)	0.00150137	Carbonate margin

Table 10 Evapotranspiraiton estimates from lithological surfaces relevant to the southeastern margin of Salar de Atacama.

Appendix S9: Applicability of model boundary & initial conditions to Salar de Atacama

As described in section 1.5.1, the 2-D model's boundary conditions were based on reflecting hydrologic conditions for both arid basins generally and SdA specifically. For modeling the topography, developing a reproducible model that was relevant to SdA as well as other arid basins was the motivation for relying on SdA's elevation data. A curve of best fit was created for modeling the cross section's topography in order to smooth out the model's surface and thus remove any potential computational errors. The bottom of the model is at to 2,000 masl; the model's lowest surface at the modeled salar nucleus is at 2,300 masl.

Regarding the distribution of the modeled hydrologic conditions, it has been widely documented that little recharge from precipitation occurs in arid basins such as SdA (Corenthal et al., 2016; Tyler et al., 2006); surficial recharge was therefore not included as a boundary condition. Thus all other boundaries not otherwise described in section 1.5.1 have no flux of either fluid or solute. The initiation of the model holds particular difficulty in applicability to real conditions. It is recognized that the initial condition of no solute concentration is not realistic for an initial condition of a brine-dominant aquifer; however, given that the focus of the study is on the time period after reaching the initial steady state, the initial conditions do not impact the results of this modeling methodology. Furthermore, an exercise of setting the initial conditions for the entire aquifer as brine (200 $g \bullet cm^{-3}$) had similar results compared to its freshwater

counterpart. Therefore, the issue of initial solute conditions is nullified by the process of reviewing results of the models after they have reached their initial dynamic steady state.

All iterations run with the above-described initial conditions to 3,000,000 days, which represents a point when both the homogenous and the heterogeneous models of SdA's hydrostratigraphy reach a dynamic steady state based on the total mass of solute in the model changing less than 0.01% consistently for 50,000 years, as illustrated in figure 23.

It is important to note that a level of uncertainty remains in the full impact of geologic heterogeneity when the above-mentioned factors remain homogenous, considering that heterogeneous hydraulic conductivity would inherently have heterogeneous dispersion values as well. However, these values remain consistent for the sake of eliminating potential computational errors; calculating the correct dispersion values at this scale would also be implausible.

A series of sensitivity analyses were conducted on the above-described hydrologic parameters. The sensitivity analyses consisted of testing changes in both ET and inflow on the response of the interface in homogenous, isotropic conditions. These analyses served to constrain the amount of numerical control the boundary conditions had on the interface's modeled sensitivity. Based on the sensitivity analyses of inflow, the model is not sensitive to the lateral distribution of inflow; rather, groundwater flow and the corresponding interface location and geometry primarily responds to inflow rates regardless of its distribution. However, sensitivity analyses of ET indicate that both the distribution and the rate of ET impact near surface flow dynamics.

REFERENCES

Anderson, M., Low, R., & Foot, S. (2002). Sustainable groundwater development in arid, high Andean basins. *Geological Society, London, Special Publications*, *193*(1), 133–144. https://doi.org/10.1144/GSL.SP.2002.193.01.11

Bailey, R. T. (2015). Quantifying transient post-overwash aquifer recovery for atoll islands in the Western Pacific. *Hydrological Processes*, *29*(20), 4470–4482. https://doi.org/10.1002/hyp.10512

Bascuñán, S., Arriagada, C., Le Roux, J., & Deckart, K. (2016). Unraveling the Peruvian Phase of the Central Andes: Stratigraphy, sedimentology and geochronology of the Salar de Atacama Basin (22°30-23°S), northern Chile. *Basin Research*, *28*(3), 365–392. https://doi.org/10.1111/bre.12114

Betancourt, J. L. (2000). A 22,000-Year Record of Monsoonal Precipitation from Northern Chile's Atacama Desert. *Science*, *289*(5484), 1542–1546. https://doi.org/10.1126/science.289.5484.1542

Blard, P. H., Sylvestre, F., Tripati, A. K., Claude, C., Causse, C., Coudrain, A., et al. (2011). Lake highstands on the Altiplano (Tropical Andes) contemporaneous with Heinrich 1 and the Younger Dryas: New insights from 14C, U-Th dating and 18O of carbonates. *Quaternary Science Reviews*, *30*(27–28), 3973–3989. https://doi.org/10.1016/j.quascirev.2011.11.001

Blodgett, T. a., Lenters, J. D., & Isacks, B. L. (1997). Constraints on the origin of paleolake expansions in the Central Andes. *Earth Interactions*, *1*(1), 1–1. https://doi.org/10.1175/1087-3562(1997)001<0001:CotOoP>2.0.CO;2

Bobst, A. L., Lowenstein, T. K., Jordan, T. E., Godfrey, L. V., Ku, T. L., & Luo, S. (2001). A 106 ka paleoclimate record from drill core of the Salar de Atacama, northern Chile. *Palaeogeography, Palaeoclimatology, Palaeoecology*, *173*(1–2), 21–42. https://doi.org/10.1016/S0031-0182(01)00308-X

Boutt, D. F., Hynek, S. A., Munk, L. A., & Corenthal, L. G. (2016a). Rapid recharge of fresh water to the halite-hosted brine aquifer of Salar de Atacama, Chile. *Hydrological Processes*. https://doi.org/10.1002/hyp.10994

Boutt, D. F., Hynek, S. A., Munk, L. A., & Corenthal, L. G. (2016b). Rapid recharge of fresh water to the halite-hosted brine aquifer of Salar de Atacama, Chile. *Hydrological Processes*. https://doi.org/10.1002/hyp.10994

Carmona, V., Pueyo, J. J., Taberner, C., Chong, G., & Thirlwall, M. (2000). Solute inputs in the Salar de Atacama (N. Chile). *Journal of Geochemical Exploration*, *69–70*, 449–452. https://doi.org/10.1016/S0375-6742(00)00128-X

Clarke, J. D. A. (2006). Antiquity of aridity in the Chilean Atacama Desert. *Geomorphology*, *73*(1–2), 101–114. https://doi.org/10.1016/j.entcs.2005.12.035

Corenthal, L. G., Boutt, D. F., Hynek, S. A., & Munk, L. A. (2016). Regional groundwater flow and accumulation of a massive evaporite deposit at the margin of the Chilean Altiplano. *Geophysical Research Letters*, *43*(15), 8017–8025. https://doi.org/10.1002/2016GL070076

Cortecci, G., Boschetti, T., Mussi, M., Lameli, C. H., Mucchino, C., & Barbieri, M. (2005). New chemical and original isotopic data on waters from El Tatio geothermal field, northern Chile. *Geochemical Journal*, *39*(6), 547–571. https://doi.org/10.2343/geochemj.39.547

Dorsaz, J. M., Gironás, J., Escauriaza, C., & Rinaldo, A. (2013). The geomorphometry of endorheic drainage basins: Implications for interpreting and modelling their evolution. *Earth Surface Processes and Landforms*, *38*(15), 1881–1896. https://doi.org/10.1002/esp.3475

Duffy, J., & Al-Hassan, S. (1988). Groundwater circulation in a closed desert basin: topographic scaling and climatic forcing. *Water Resources Research*, *24*(10), 1675–1688.

Eugster, H. (1980). Geochemistry of evaporitic lacustrine deposits. *Annual Review of Earth and Planetary Sciences*, *8*, 35–63.

Fan, Y., & Schaller, M. F. (2009). River basins as groundwater exporters and importers: Implications for water cycle and climate modeling. *Journal of Geophysical Research Atmospheres*, *114*(4). https://doi.org/10.1029/2008JD010636

Fan, Y., Duffy, C. J., & Oliver, D. S. (1996). Density-driven groundwater flow in closed desert basins : field investigations and numerical experiments. *Journal of Hydrology*, *196*, 139–184.

Fritz, S. C., Baker, P. A., Lowenstein, T. K., Seltzer, G. O., Rigsby, C. A., Dwyer, G. S., et al. (2004). Hydrologic variation during the last 170,000 years in the southern hemisphere tropics of South America. *Quaternary Research*, *61*(1), 95–104. https://doi.org/10.1016/j.yqres.2003.08.007

Gayo, E. M., Latorre, C., Jordan, T. E., Nester, P. L., Estay, S. A., Ojeda, K. F., & Santoro, C. M. (2012). Late Quaternary hydrological and ecological changes in the hyperarid core of the northern Atacama Desert (~21??S). *Earth-Science Reviews*, *113*(3–4), 120–140. https://doi.org/10.1016/j.earscirev.2012.04.003

Gelhar, L. W., Welty, C., & Rehfeldt, K. R. (1992). A Critical Review of Data on Field-Scale Dispersin in Aquifers. *Water Resources Research*, *28*(7), 1955–1974. https://doi.org/10.1029/92WR00607

Godfrey, L. V., Jordan, T. E., Lowenstein, T. K., & Alonso, R. L. (2003). Stable isotope constraints on the transport of water to the Andes between 22?? and 26??S during the last glacial cycle. *Palaeogeography, Palaeoclimatology, Palaeoecology*, *194*(1–3), 299–317. https://doi.org/10.1016/S0031-0182(03)00283-9

Haitjema, H. M., & Mitchell-Bruker, S. (2005). Are water tables a subdued replica of the topography? *Ground Water*, *43*(6), 781–786. https://doi.org/10.1111/j.1745-6584.2005.00090.x

Hamann, E., Post, V., Kohfahl, C., Prommer, H., & Simmons, C. T. (2015). Numerical investigation of coupled density-driven flow and hydrogeochemical processes below playas. *Water Resources Research*, *51*(11), 9338–9352. https://doi.org/10.1002/2015WR017833

Harbaugh, Arlen, W. (2005). MODFLOW-2005 , The U . S . Geological Survey Modular Ground-Water Model — the Ground-Water Flow Process. *U.S. Geological Survey Techniques and Methods*, 253. https://doi.org/U.S. Geological Survey Techniques and

Hartley, A., Chong, G., Houston, J., & Mather, A. (2005). 150 million years of climatic stability: evidence from the Atacama Desert, northern Chile. *Journal of the Geological Society*, *162*(3), 421–424. https://doi.org/10.1144/0016-764904-071

Hartley, A. J., & Chong, G. (2002). Late Pliocene age for the Atacama Desert: Implications for the desertification of western South America. *Geology*, *30*(1), 43–46. https://doi.org/10.1130/0091-7613(2002)030<0043:LPAFTA>2.0.CO;2

Heiss, J. W., & Michael, H. A. (2014). Saltwater-freshwater mixing dynamics in a sandy beach aquifer over tidal, spring-neap, and seasonal cycles. *Water Resources Research*, *50*, 6747–6766. https://doi.org/10.1002/2015WR017273.Received

Herrera, C., Custodio, E., Chong, G., Lambán, L. J., Riquelme, R., Wilke, H., et al. (2016). Groundwater flow in a closed basin with a saline shallow lake in a volcanic area: Laguna Tuyajto, northern Chilean Altiplano of the Andes. *Science of the Total Environment*, *541*, 303–318. https://doi.org/10.1016/j.scitotenv.2015.09.060

Houston, J. (2006a). Evaporation in the Atacama Desert: An empirical study of spatio-temporal variations and their causes. *Journal of Hydrology*, *330*(3–4), 402–412. https://doi.org/10.1016/j.jhydrol.2006.03.036

Houston, J. (2006b). The great Atacama flood of 2001 and its implications for Andean hydrology. *Hydrological Processes*, *20*(3), 591–610. https://doi.org/10.1002/hyp.5926

Houston, J. (2009). A recharge model for high altitude, arid, Andean aquifers. *Hydrological Processes*, *23*(16), 2383–2393. https://doi.org/10.1002/hyp.7350

Houston, J., Butcher, A., Ehren, P., Evans, K., & Godfrey, L. (2011). The evaluation of brine prospects and the requirement for modifications to filing standards. *Economic Geology*, *106*(7), 1125–1239. https://doi.org/10.2113/econgeo.106.7.1225

Jayne, R. S., Pollyea, R. M., Dodd, J. P., Olson, E. J., & Swanson, S. K. (2016). Spatial and temporal constraints on regional-scale groundwater flow in the Pampa del Tamarugal Basin, Atacama Desert, Chile. *Hydrogeology Journal*, (August), 1921–1937. https://doi.org/10.1007/s10040-016-1454-3

Jordan, T. E., Munoz, N., Hein, M., Lowenstein, T., Godfrey, L., & Yu, J. (2002). Active faulting and folding without topographic expression in an evaporite basin, Chile. *Bulletin of the Geological Society of America*, *114*(11), 1406–1421. https://doi.org/10.1130/0016-7606(2002)114<1406:AFAFWT>2.0.CO;2

Jordan, T. E., Mpodozis, C., Muñoz, N., Blanco, N., Pananont, P., & Gardeweg, M. (2007). Cenozoic subsurface stratigraphy and structure of the Salar de Atacama Basin, northern Chile. *Journal of South American Earth Sciences*, *23*(2–3), 122–146. https://doi.org/10.1016/j.jsames.2006.09.024

Kampf, S. K., & Tyler, S. W. (2006). Spatial characterization of land surface energy fluxes and uncertainty estimation at the Salar de Atacama, Northern Chile. *Advances in Water Resources*, *29*(2), 336–354. https://doi.org/10.1016/j.advwatres.2005.02.017

Kampf, S. K., Tyler, S. W., Ortiz, C. A., Muñoz, J. F., & Adkins, P. L. (2005). Evaporation and land surface energy budget at the Salar de Atacama, Northern Chile. *Journal of Hydrology*,

310(1–4), 236–252. https://doi.org/10.1016/j.jhydrol.2005.01.005

Konikow, L. F., Akhavan, M., Langevin, C. D., Michael, H. A., & Sawyer, A. H. (2013). Seawater circulation in sediments driven by interactions between seabed topography and fluid density. *Water Resources Research*, *49*(3), 1386–1399. https://doi.org/10.1002/wrcr.20121

Langevin, C. D., & Guo, W. (2006). MODFLOW / MT3DMS – Based Simulation of Variable-Density Ground Water Flow and Transport, *44*(3), 339–351. https://doi.org/10.1111/j.1745-6584.2005.00156.x

Lindsay, J. M., De Silva, S., Trumbull, R., Emmermann, R., & Wemmer, K. (2001). La Pacana caldera, N. Chile: A re-evaluation of the stratigraphy and volcanology of one of the world's largest resurgent calderas. *Journal of Volcanology and Geothermal Research*, *106*(1–2), 145–173. https://doi.org/10.1016/S0377-0273(00)00270-5

Liu, Y., Mao, X., Chen, J., & Barry, D. A. (2014). Influence of a coarse interlayer on seawater intrusion and contaminant migration in coastal aquifers. *Hydrological Processes*, *28*(20), 5162–5175. https://doi.org/10.1002/hyp.10002

Lowenstein, T. K., Hein, M. C., Bobst, A. L., Jordan, T. E., Ku, T.-L., & Luo, S. (2003). An Assessment of Stratigraphic Completeness in Climate-Sensitive Closed-Basin Lake Sediments: Salar de Atacama, Chile. *Journal of Sedimentary Research*, *73*(1), 91–104. https://doi.org/10.1306/061002730091

Mardones, L. (1986). Características geológicas e hidrogeológicas del Salar de Atacama. *El Litio: Un Nuevo Recurso Para Chile*.

Maxey, G. B. (1968). Hydrogeology of Desert Basins. *Groundwater*, *6*(5), 10–22. https://doi.org/10.1111/j.1745-6584.1968.tb01660.x

McCartney, J. (2001). Hydraulic and Hydrochemical Interactions in the Tilopozo Groundwater Zone Salar de Atacama Region II , Chile (Master's thesis).

Meng, G.-I., Han, Y., Wang, S., & Wang, Z. (2002). Seawater Intrusion Types and Regional Divisions in the Southern Coast of Laizhou Bay ". *Chinese Journal of Oceanology and Limnology*, *20*(3), 277–284.

Michael, H. A., & Khan, M. R. (2016). Impacts of physical and chemical aquifer heterogeneity on basin-scale solute transport: Vulnerability of deep groundwater to arsenic contamination in Bangladesh. *Advances in Water Resources*, *98*, 147–158. https://doi.org/10.1016/j.advwatres.2016.10.010

Michael, H. A., Scott, K. C., Koneshloo, M., Yu, X., Khan, M. R., & Li, K. (2016). Geologic influence on groundwater salinity drives large seawater circulation through the continental shelf. *Geophysical Research Letters*, *43*(20), 10,782-10,791. https://doi.org/10.1002/2016GL070863

Montgomery, E. L., Rosko, M. J., Castro, S. O., Keller, B. R., & Bevacqua, P. S. (2003). Interbasin underflow between closed altiplano basins in chile. *Ground Water*, *41*(4), 523–531. https://doi.org/10.1111/j.1745-6584.2003.tb02386.x

Morgan, L. K., Werner, A. D., & Simmons, C. T. (2012). On the interpretation of coastal aquifer water level trends and water balances: A precautionary note. *Journal of Hydrology*, *470–*

471, 280–288. https://doi.org/10.1016/j.jhydrol.2012.09.001

Mpodozis, C., Arriagada, C., Basso, M., Roperch, P., Cobbold, P., & Reich, M. (2005). Late Mesozoic to Paleogene stratigraphy of the Salar de Atacama Basin, Antofagasta, Northern Chile: Implications for the tectonic evolution of the Central Andes. *Tectonophysics*, *399*(1–4 SPEC. ISS.), 125–154. https://doi.org/10.1016/j.tecto.2004.12.019

Munk, L. A., Hynek, S. A., Bradley, D., Boutt, D. F., Labay, K., & Jochens, H. (2016). Lithium brines: A global perspective. *Reviews in Economic Geology*, *18*(June), 339–365.

Philip, J., & van Duijn, C. (1996). Slumping of brine mounds: bounds on behaviour. *Journal of Hydrology*, *179*, 159–180.

Placzek, C., Quade, J., Betancourt, J. L., Patchett, P. J., Rech, J. A., Latorre, C., et al. (2009). Climate in the dry central Andes over geologic, millenial, and interannual timescale. *Annals of the Missouri Botanical Garden*, *96*(3), 386–397. https://doi.org/10.3417/2008019

Post, V., Kooi, H., & Simmons, C. (2007). Using Hydraulic Head Measurements in Variable-Density Ground Water Flow Analyses. *Ground Water*, *45*(6), 664–671. https://doi.org/10.1111/j.1745-6584.2007.00339.x

Qureshi, A. S. (2011). Water Management in the Indus Basin in Pakistan: Challenges and Opportunities. *Mountain Research and Development*, *31*(3), 252–260. https://doi.org/10.1659/MRD-JOURNAL-D-11-00019.1

Reutter, K. J., Charrier, R., Gotze, H. J., Schurr, B., Wigger, P., Scheuber, E., et al. (2006). The Salar de Atacama Basin: a Subsiding Block within the Western Edge of the Altiplano-Puna Plateau. *Andes: Active Subduction Orogeny*, 303–325. https://doi.org/10.1007/978-3-540-48684-8_14

Rissmann, C., Leybourne, M., Benn, C., & Christenson, B. (2015). The origin of solutes within the groundwaters of a high Andean aquifer. *Chemical Geology*, *396*, 164–181. https://doi.org/10.1016/j.chemgeo.2014.11.029

Rosen, M. R. (1994). The importance of groundwater in playas: A review of playa classifications and the sedimentology and hydrology of playas. *Geological Society of America Special Papers*, *289*(January 1994), 1–18. https://doi.org/10.1130/SPE289-p1

Russoniello, C. J., Fernandez, C., Bratton, J. F., Banaszak, J. F., Krantz, D. E., Andres, A. S., et al. (2013). Geologic effects on groundwater salinity and discharge into an estuary. *Journal of Hydrology*, *498*, 1–12. https://doi.org/10.1016/j.jhydrol.2013.05.049

Saez, A., Godfrey, L. V., Herrera, C., Chong, G., & Pueyo, J. J. (2016). Timing of wet episodes in Atacama Desert over the last 15 ka. The Groundwater Discharge Deposits (GWD) from Domeyko Range at 25??S. *Quaternary Science Reviews*, *145*(June), 82–93. https://doi.org/10.1016/j.quascirev.2016.05.036

Sawyer, A. H., Kaplan, L. A., Lazareva, O., & Michael, H. . (2014). Hydrologic dynamics and geochemical responses within a floodplain aquifer and hyporheic zone during Hurricane Sandy. *Water Resources Research*, *50*, 4877–4892. https://doi.org/10.1002/2013WR014222.Received

Scanlon, B., Keese, K., Flint, A., Flint, L., Gaye, C., Edmunds, W. M., & Simmers, I. (2006). Global synthesis of groundwater recharge in semiarid and arid regions. *Hydrological*

Processes, *20*(November 2006), 3335–3370. https://doi.org/10.1002/hyp

Schmitt, A. K. (2001). Gas-saturated crystallization and degassing in large-volume, crystal-rich dacitic magmas from the Altiplano-Puna, northern Chile. *Journal of Geophysical Research: Solid Earth*, *106*(B12), 30561–30578. https://doi.org/10.1029/2000JB000089

de Silva, S. L. (1989). Geochronology and stratigraphy of the ignimbrites from the 21°30'S to 23°30'S portion of the Central Andes of northern Chile. *Journal of Volcanology and Geothermal Research*, *37*(2), 93–131. https://doi.org/10.1016/0377-0273(89)90065-6

Skrzypek, G., Dogramaci, S., Rouillard, A., & Grierson, P. F. (2016). Groundwater seepage controls salinity in a hydrologically terminal basin of semi-arid northwest Australia. *Journal of Hydrology*, *542*, 627–636. https://doi.org/10.1016/j.jhydrol.2016.09.033

Tejeda, I., Cienfuegos, R., Muñoz, J. F., & Durán, M. (2003). Numerical Modeling of Saline Intrusion in Salar de Atacama. *Journal of Hydrologic Engineering*, *8*(1), 25. https://doi.org/10.1061/(ASCE)1084-0699(2003)8:1(25)

Trabelsi, F., Mammou, A. Ben, Tarhouni, J., Piga, C., & Ranieri, G. (2013). Delineation of saltwater intrusion zones using the time domain electromagnetic method: The Nabeul-Hammamet coastal aquifer case study (NE Tunisia). *Hydrological Processes*, *27*, 2004–2020. https://doi.org/10.1002/hyp.9354

Tyler, S. W., Muñoz, J. F., & Wood, W. W. (2006). The response of playa and sabkha hydraulics and mineralogy to climate forcing. *Ground Water*. https://doi.org/10.1111/j.1745-6584.2005.00096.x

Vásquez, C., Ortiz, C., Suárez, F., & Muñoz, J. F. (2013). Modeling flow and reactive transport to explain mineral zoning in the Atacama salt flat aquifer, Chile. *Journal of Hydrology*, *490*, 114–125. https://doi.org/10.1016/j.jhydrol.2013.03.028

Vuille, M., & Ammann, C. (1997). Regional snowfall patterns in the high, arid Andes. *Climatic Change*, *36*, 413–423. https://doi.org/10.1007/978-94-015-8905-5_10

Wang, J., Song, C., Reager, J. T., Yao, F., Famiglietti, J. S., Sheng, Y., et al. (2018). Recent global decline in endorheic basin water storages. *Nature Geoscience*, *11*(December). https://doi.org/10.1038/s41561-018-0265-7

Wooding, R., Tyler, S. W., & White, I. (1997). Convection in groundwater below an evaporating salt lake : 1 . Onset of instability. *Water Resources Research*, *33*(6), 1199–1217.

Wurtsbaugh, W. A., Miller, C., Null, S. E., Derose, R. J., Wilcock, P., Hahnenberger, M., et al. (2017). Decline of the world's saline lakes. *Nature Publishing Group*, *10*(11), 816–823. https://doi.org/10.1038/ngeo3052

Xiao, D., Jiang, S., Thul, D., Huang, W., Lu, Z., & Lu, S. (2017). Combining rate-controlled porosimetry and NMR to probe full-range pore throat structures and their evolution features in tight sands : A case study in the Songliao Basin , China. *Marine and Petroleum Geology*, *83*, 111–123. https://doi.org/10.1016/j.marpetgeo.2017.03.003

Yager, R. M., McCoy, K. J., Voss, C. I., Sanford, W. E., & Winston, R. B. (2017). The Role of Uplift and Erosion in the Persistence of Saline Groundwater in the Shallow Subsurface. *Geophysical Research Letters*. https://doi.org/10.1002/2017GL072980

Ye, M., Wang, L., Pohlmann, K. F., & Chapman, J. B. (2016). Evaluating Groundwater Interbasin Flow Using Multiple Models and Multiple Types of Data. *Ground Water*, *54*(6), 1–13. https://doi.org/10.1111/gwat.12422

Yechieli, Y. (2000). Fresh-Saline Ground Water Interface in the Western Dead Sea Area. *Ground Water*. https://doi.org/10.1111/j.1745-6584.2000.tb00253.x

Yechieli, Y., Kafri, U., Goldman, M., & Voss, C. I. (2001). Factors controlling the configuration of the fresh-saline water interface in the Dead Sea coastal aquifers: Synthesis of TDEM surveys and numerical groundwater modeling. *Hydrogeology Journal*, *9*(4), 367–377. https://doi.org/10.1007/s100400100146

Zhu, C., Waddell, R. K., Star, I., & Ostrander, M. (1998). Responses of ground water in the Black Mesa basin, northeastern Arizona, to paleoclimatic changes during the late Pleistocene and Holocene. *Geology*, *26*(2), 127–130. https://doi.org/10.1130/0091-7613(1998)026<0127:ROGWIT>2.3.CO;2